NAVAL POSTGRADUATE SCHOOL
Monterey, California

THESIS

TWO-D HEAT TRANSFER THROUGH POROUS MEDIA WITH HEAT GENERATION

by

Benjamin Martinez, Jr.

June 1984

Thesis Advisor:

Approved for public release; distribution unlimited.

T223013

REPORT DOCUMENTATION PAGE

READ INSTRUCTIONS BEFORE COMPLETING FORM

1. REPORT NUMBER
2. GOVT ACCESSION NO.
3. RECIPIENT'S CATALOG NUMBER

4. TITLE (and Subtitle)

Two-D Heat Transfer Through Porous Media with Heat Generation

5. TYPE OF REPORT & PERIOD COVERED
Engineer's Thesis; June 1984

6. PERFORMING ORG. REPORT NUMBER

7. AUTHOR(s)

Benjamin Martinez, Jr.

8. CONTRACT OR GRANT NUMBER(s)

9. PERFORMING ORGANIZATION NAME AND ADDRESS

Naval Postgraduate School
Monterey, California 93943

10. PROGRAM ELEMENT, PROJECT, TASK AREA & WORK UNIT NUMBERS

11. CONTROLLING OFFICE NAME AND ADDRESS

Naval Postgraduate School
Monterey, California 93943

12. REPORT DATE
June 1984

13. NUMBER OF PAGES
135

14. MONITORING AGENCY NAME & ADDRESS(if different from Controlling Office)

15. SECURITY CLASS. (of this report)
Unclassified

15a. DECLASSIFICATION/DOWNGRADING SCHEDULE

16. DISTRIBUTION STATEMENT (of this Report)

Approved for public release; distribution unlimited.

17. DISTRIBUTION STATEMENT (of the abstract entered in Block 20, if different from Report)

18. SUPPLEMENTARY NOTES

19. KEY WORDS (Continue on reverse side if necessary and identify by block number)

Combustion	Porous Media
Heat Transfer	Darcy Flow
Carbon	Semenov Model

20. ABSTRACT (Continue on reverse side if necessary and identify by block number)

This investigation develops an axisymmetric heat transfer-combustion model of a porous medium within a circular cylinder. System flow is governed by Darcy's law. Carbon and air properties are treated as variables of temperature. A combined continuity-Darcy equation, an oxygen mass balance equation, and energy balance equations (one each) for air and carbon, describe the conservation laws of the system. Transport mechanisms for

#20 - ABSTRACT - CONTINUED

oxygen mass transfer are molecular diffusion and convective transport, and an oxygen consumption term to account for combustion is included. Heat transfer mechanisms included in the model are conduction and convection. Radiation is accounted for at applicable boundaries only. Nonvolatile combustion is accounted for in the carbon energy and oxygen mass balance equations as a heat generation term of Arrhenius type. The numerical solution of four coupled, nonlinear, transient partial differential field equations is accomplished using the Galerkin formulation of the Finite Element Method. The effect of porosity on system behavior is examined.

Approved for public release; distribution unlimited.

Two-D Heat Transfer Through Porous Media with Heat Generation

by

Benjamin Martinez, Jr.
Lieutenant, United States Navy
B.A., Trinity University, 1974

Submitted in partial fulfillment of the
requirements for the degrees of

MASTER OF SCIENCE IN MECHANICAL ENGINEERING
and
MECHANICAL ENGINEER

from the

NAVAL POSTGRADUATE SCHOOL

June 1984

ABSTRACT

This investigation develops an axisymmetric heat transfer-combustion model of a porous medium within a circular cylinder. System flow is governed by Darcy's law. Carbon and air properties are treated as variables of temperature. A combined continuity-Darcy equation, an oxygen mass balance equation, and energy balance equations (one each) for air and carbon, describe the conservation laws of the system. Transport mechanisms for oxygen mass transfer are molecular diffusion and convective transport, and an oxygen consumption term to account for combustion is included. Heat transfer mechanisms included in the model are conduction and convection. Radiation is accounted for at applicable boundaries only. Nonvolatile combustion is accounted for in the carbon energy and oxygen mass balance equations as a heat generation term of Arrhenius type. The numerical solution of four coupled, nonlinear, transient partial differential field equations is accomplished using the Galerkin formulation of the Finite Element Method. The effect of porosity on system behavior is examined.

Thesis
M3592
c.1

TABLE OF CONTENTS

I. INTRODUCTION ---------- 14

A. PRIOR INVESTIGATIONS ---------- 14

II. PROBLEM DESCRIPTION ---------- 19

III. THEORY AND BACKGROUND ---------- 21

A. DESCRIPTION OF THE POROUS MEDIUM ---------- 21

B. DARCY'S LAW AND PORE VELOCITY ---------- 24

C. SEMENOV MODEL OF COMBUSTION ---------- 27

D. ARRHENIUS LAW OF REACTION RATES ---------- 28

E. CARBON HEAT TRANSFER EQUATION FOR POROUS MEDIA ---------- 32

F. HEAT TRANSFER EQUATION FOR AIR IN POROUS MEDIA ---------- 33

G. OXYGEN DIFFUSION EQUATION FOR POROUS MEDIA --- 34

H. BOUNDARY CONDITIONS ---------- 36

I. INITIAL CONDITIONS ---------- 41

IV. NUMERICAL CONSIDERATIONS ---------- 46

A. TREATMENT OF NONLINEAR COMBUSTION TERM ------- 46

1. Excitation (Force) Term Treatment -------- 46

2. Linear Operator Treatment of O_2 Concentration ---------- 47

3. Bilinear Operator Treatment of O_2 and TC - 48

B. OPTIMAL COMPACT STORAGE (OCS) ---------- 49

C. GRID CONVERGENCE ---------- 49

D. MODEL VALIDATION TESTS ---------- 51

1. The Steady State Problem ---------- 51

2. The Finite Slab ---------- 52

3. The Cylinder ---------- 53

4. Multidimensional Solutions by the Product Method ---------- 54

5. Validation Problem ---------- 56

6. Testing the Model's Ability to Accept and Reject Heat ---------- 57

7. The One Dimensional Problem ---------- 58

V. DISCUSSION AND CONCLUSIONS ---------- 77

A. BOUNDARY CONDITIONS ---------- 77

B. EXCITATIONS ---------- 78

C. PHYSICAL CHARACTERISTICS OF THE SYSTEM ------ 78

D. POROSITY ANALYSIS ---------- 79

E. CONCLUSIONS ---------- 81

F. RECOMMENDATIONS ---------- 81

APPENDIX A: FORMULATION OF FIELD EQUATIONS ---------- 87

A. PRESSURE DISTRIBUTION EQUATION ---------- 87

B. POROUS SOLID HEAT TRANSFER EQUATION --------- 88

C. AIR HEAT TRANSFER EQUATION ---------- 90

D. OXYGEN MOLECULE DIFFUSION EQUATION ---------- 100

APPENDIX B: AUXILIARY EQUATION FORMULATION ---------- 104

A. CONTINUITY EQUATION ---------- 104

B. LAGRANGE POLYNOMIAL APPROXIMATIONS FOR THERMAL PROPERTIES ---------- 104

C. CARBON PARTICLE SURFACE RECESSION ---------- 105

APPENDIX C: GALERKIN FEM FORMULATION ---------- 107

A. FINITE ELEMENT METHOD ---------- 107

1. Galerkin Formulation ---------- 107

2. Implementation of Boundary Conditions ---- 117

3. Treatment of the Reaction Rate Term ------ 118

4. Implementation of Reaction Term in the Numerical Method ---------- 121

5. Derivation of the FEM Operators ---------- 123

LIST OF REFERENCES ---------- 132

INITIAL DISTRIBUTION LIST ---------- 135

LIST OF FIGURES

3.1 Geometric Model of Porous Medium ---------- 43

3.2 Top View of Radial Convection Circuit ---------- 44

3.3 Electrical Analogy of Thermal Circuit at $r/r_o = 1.0$ ---------- 45

4.1 Classical Transient 1-D Geometries ---------- 60

4.2 Illustration of the Product Technique ---------- 61

4.3 Sample Problem, Cylinder Geometry ---------- 62

4.4 Grid Effects at Point A, (0,0) ---------- 63

4.5 Grid Effects at Point B, (0,1) ---------- 64

4.6 Grid Effects at Point C, (1,1) ---------- 65

4.7 Grid Effects at Point D, (1,0) ---------- 66

4.8 Grid Effects at Point E, (.5,.5) ---------- 67

4.9 Model Accepting Heat (Carbon Temperature Profile) ---------- 68

4.10 Model Rejecting Heat (Carbon Temperature Profile) ---------- 69

4.11 Model Accepting Heat (Oxygen Concentration Profile) ---------- 70

4.12 Model Rejecting Heat (Oxygen Concentration Profile) ---------- 71

4.13 Accept/Reject Heat Problem Input Data Set -------- 72

4.14 One Dimensional Problem (Carbon Temperature Profile and Oxygen Concentration Profile) -------- 73

4.15 One Dimensional Problem (Carbon Temperature Profile) ---------- 74

4.16 One Dimensional Problem (Oxygen Temperature Profile) ---------- 75

4.17 One Dimensional Problem Data Set ---------- 76

5.1 Carbon Temperature Profile (Porosity = 0.476) Radial Heat Flux (Out) 50-Btu/ft^2-hr ---------- 83

5.2 Oxygen Concentration (porosity = 0.476) Radial Heat Transfer (Out) 50-Btu/ft^2-hr ------- 84

5.3 Maximium Carbon Temperature Summary Porosity --- 85

5.4 Oxygen Concentration Profile Summary Porosity -- 86

A.1 Separating A Differential Volume of Porous Medium into Respective Volumes of Solid and Air ---------- 103

C.1 Area Interpolation Functions ---------- 129

C.2 Area Coordinates ---------- 130

C.3 Local Coordinates ---------- 131

LIST OF SYMBOLS

A -- Arrhenius coefficient, wetted surface area

$\underset{\approx}{A}$ -- Stiffness matrix

$\underset{\approx}{B}$ -- Mass matrix

c -- Specific heat at constant pressure

D -- Unit cell dimension

$\mathcal{D}$ -- Mass diffusion coefficient

d -- Particle diameter

E -- Activation energy

e -- Specific internal energy

F -- Fraction

$\underset{\sim}{F}$ -- Excitation vector

f -- Stoichiometric ratio

G -- Pseudo mass velocity

g -- Gravitational constant

ΔH -- Heat of combustion

h -- Convection heat transfer coefficient

h -- Specific enthalpy

K -- Constant

k -- Thermal Conductivity

L -- Thickness of porous medium

ℓ_e -- Element length

M -- Molecular weight

m -- Specific permeability

n -- Reaction order

N_j -- Global Basis Function

P -- Pressure

Pr -- Prandtl number

p -- Porosity

Q -- Filter velocity

q -- Heat generation or loss

q' -- Heat flux

R -- Reaction rate

R' -- Rate per unit area

$\mathcal{R}$ -- Gas constant

Re -- Reynolds number

r -- Radial coordinate

R_i -- Residual function

T -- Temperature

$\hat{T}$ -- Absolute temperature

t -- Time

t^*_{n-1} -- Previous time step

U -- Internal energy

u -- Pore velocity, radial

v -- Pore velocity, axial

V -- Void volume, molecular volume

z -- Axial coordinate

Z -- Specific internal area

Greek Symbols

α -- Thermal diffusivity

δ -- Pore diameter

δ^K -- Kronecker delta function

ε -- Thermal emissivity

θ -- Solution coefficient

Λ -- Field operator

μ -- Dynamic viscosity

ξ -- Local element coordinate

ρ -- Mass density

σ -- Stefan-Boltzman constant

τ -- Tortuosity, stress

ϕ -- Oxygen concentration

ψ -- Particle shape factor, approximate solution

Subscripts

a -- Air

c -- Carbon

CO -- Carbon monoxide

CO_2 -- Carbon dioxide

e -- Effective

fm -- Film

g -- Heat generation

i -- At the current time or step

ig -- Ignition

o -- Cylinder dimension (i.e., r_o is cylinder radius, z_o is cylinder length)

O_2 -- Oxygen

p -- At constant pressure

r -- Radiation

s -- Solid

st -- Starting

u -- Universal

∞ -- Ambient conditions

I. INTRODUCTION

A. PRIOR INVESTIGATIONS

The problem of characterizing physical systems involving combustion and quantifying the accompanying thermal response has received attention in recent years. The level of difficulty encountered in a problem of this type precluded analytical as well as numerical solutions. The difficulty of the problem lies in the number of disciplines that encompass it. The problem involves the kinetics of combustion, heat and mass transfer mechanisms and fluid flow. Numerical solutions with increased efficiency in computation are now possible with high speed computers.

The combustion problem has applications in the areas of forest fire control, energy conservation, underground (nuclear) fuel storage and waste disposal, and natural gas fire control. Major contributions may be made in the area of energy production and conservation by the analysis of heat generation and ignition characteristics of combustible materials.

The characterization of combustion and heat transfer in porous media has been of particular interest. A brief survey of some of the investigations in the area of combustion and heat transfer in porous media follows. The intent is to acquaint the reader with work in the field that offered insight into the formulation of this investigation.

Investigations by Kordylewski on the influence of aerodynamics on the critical parameters of thermal ignition [Ref. 1], examined homogeneous combustion in a two-dimensional cylindrical reactor. The transient analysis involved Arrhenius combustion of a solid fuel. Heat transfer mechanisms considered were convection and conduction. Because the investigation dealt with thermal ignition theory, reactant consumption was omitted. The flow field was assumed to be steady prior to ignition and constant fluid properties were assumed.

Safety dictates the assessment of the structural integrity of a building after a severe fire. In order to predict stresses due to fire in buildings, the thermal response must be known. Sahota and Pagni [Ref. 2], formulated a transient solution for two-phase, two-component flow in one-dimensional porous concrete structures. The mechanisms considered included: heat conduction, molecular diffusion of gaseous components, and pressure-driven convective flow subject to Darcy's law.

A sudden reduction in feed temperature in a packed-bed reactor leads to the transient temperature rise known as "wrong-way behavior." This behavior was investigated by Mehta, Sams, and Luss [Ref. 3]. The work identifies the important rate processes and parameters which cause the behavior, and generates an expression for predicting the magnitude of the maximum transient temperature.

Ignition parameters in porous solid fuels have been analyzed by Kim and Chung [Ref. 4]. They investigated three porous solid fuel geometries (a semi-infinite slab, an infinitely long circular cylinder and a sphere) with constant energy and gaseous oxidant fluxes at the fuel surface. Laplace transformation of the nondimensionalized oxidant mass equation and fuel energy equation allowed for asymptotic solution of a nondimensionalized transient temperature equation which is valid in the neighborhood of the fuel surface. Observations included shorter ignition times for spheres compared to slabs. Times for ignition increased with fuel size and approached values of semi-infinite slabs asymptotically. Other effects of size and geometry of porous solid fuels on ignition parameters are presented.

Saatdjian and Caltagirone [Ref. 5] investigated a transient two-dimensional combustion model with natural convection. A porous medium undergoing exothermic combustion was saturated by a gas and bounded by two impermeable planes. Permeability, fluid viscosity, thermal conductivity of the porous medium, and the heat of reaction were assumed to be constants.

Horne and O'Sullivan [Ref. 6], Hickox [Ref. 7] and Chan and Banerjee [Ref. 8], investigated the natural convection phenomenon in porous media. Exothermic reactions were not addressed in these investigations. Horne and O'Sullivan considered the effects of variable viscosity on the stability of a porous layer in a transient two-dimensional problem.

The boundary configuration for this work was a two-dimensional region with a line of vertical symmetry, enclosed on both sides by impermeable, insulated sidewalls, and heated along half of the base. The convective flow of fluid through porous media heated from below has applications in the study of behavior of geothermal systems. Hickox studied convection as an application to sub-seabed disposal of nuclear waste. The problem was a two-dimensional transient analysis of free convection produced by a concentrated heat source (implanted container of waste material) in the subsurface sedimentary layer of a seabed. The porous medium was assumed to be rigid, homogeneous and isotropic. Density changes of the fluid were accounted for only in the buoyancy term of Darcy's law. Permeability, viscosity and thermal conductivity were assumed to be constant. Chan and Banerjee conducted a transient three-dimensional analysis of natural convection in porous media. In addition to convective heat transfer, conduction was also considered between solid spherical particles that comprise the porous medium. The porous medium was considered homogeneous and isotropic in its physical properties including permeability and thermal conductivity, both of which were assumed to be constant with temperature. Fluid density was considered to be constant except in the buoyancy term of Darcy's law.

In 1982, Vatikiotis [Ref. 9] considered a transient one-dimensional heat transfer and combustion model of a porous

medium. The heat transfer mechanisms included were conduction, convection and radiation. One problem considered was a porous mat subject to Arrhenius combustion in which all properties were temperature dependent. The capillary serial (permeability) model introduced by Scheidegger [Ref. 10] was employed.

The current investigation considers the effects of porosity on system behavior for a two-dimensional (axisymmetric) model of combustion in a porous medium. A great part of the following analysis may be found in Vatikiotis [Ref. 9]. The pertinent parts are repeated here for convenience to the reader. Deviations are cited and are for the most part due to the axisymmetric two-dimensional aspect of the present model vice the previous one-dimensional model. The storage scheme employed by the numerical model warrants the reader's attention. The savings in computer storage realized by utilizing the method of Franke and Salinas [Ref. 29], is substantial and is addressed in the Numerical Section of this work. The nonlinear combustion term is treated as a bilinear spatial operator of carbon temperature and oxygen concentration, in contrast to the Vatikiotis treatment of the term as an excitation vector. The idea behind the present treatment was to capture the effects of the nonlinear combustion term on both of these dependent variables. It was felt that this would alleviate some numerical difficulties. A numerical model is formulated and results are presented.

II. PROBLEM DESCRIPTION

The problem under investigation is that of combustion of a porous fuel (carbon) imbedded in a cylindrical container. Pressure gradients induce convective currents through the medium. The air flow produces two opposing effects: (1) internal convective heat transfer, and (2) a supply of oxygen to promote heat generation through combustion. Extinguishment or sustained combustion of the porous medium depend on the interaction of these effects. If heat transfer dominates, the combustion will proceed to extinguishment, otherwise combustion will continue. A mathematical model was developed to provide an understanding of this interaction and its effect on thermal behavior.

The mathematical model is formulated as follows. Energy balances on the carbon and convected air provide heat transfer equations for each. The heat transfer mechanisms incorporated in the model are: (1) conduction, (2) convection and (3) radiation (where applicable, at boundaries). In addition, nonvolatile combustion is included in the carbon heat transfer equation as a fractional order heat generation term of Arrhenius type.

The conservation of species law is applied to the oxygen molecule concentration to yield a third equation. The resulting oxygen mass transfer equation includes the

transfer mechanism of: (1) molecular diffusion, and (2) convective transport of species. An oxygen consumption term due to combustion is included.

The fourth field equation involves the system pressure gradient. The equation is a combined Darcy's law and air mass continuity equation for the system.

The conservation equations describing the system field are four transient, coupled, nonlinear partial differential equations. The four equations are solved by a two-dimensional Galerkin formulation of the Finite Element Method. The integration scheme used for this highly stiff system is one presented by Gear and modified by Franke [Ref. 30]. The scheme is especially suited to systems of implicit and stiff differential equations. The integration scheme is used in conjunction with an optimal compact storage scheme proposed by Franke and Salinas [Ref. 29].

III. THEORY AND BACKGROUND

A. DESCRIPTION OF THE POROUS MEDIUM

In this work, a porous medium is considered to be a solid containing interconnecting pores that allow fluid to permeate and flow through the solid. Either of two classes of porous media, consolidated (solid and rigid) and unconsolidated (comprised of discrete particles as found in granular beds) may be considered. Each class of porous media may have isotropic nonhomogeneous properties.

The common characteristics of all porous media are: (1) porosity, (2) specific internal area, (3) pore diameter, and (4) tortuosity. Porosity, p, is defined as the ratio of void volume to total volume. The specific internal area, Z, is the ratio of internal surface area to bulk volume. In general, the distribution of pore size in a porous medium is random (nonhomogeneous) and dynamic (subject to small strains induced by the transient pressure field). The situation motivates the investigator to treat the porous medium as a continuum possessing idealistic geometrical properties of porosity and pore diameter. The specific internal area is obtained from the porosity model. Though many conventions exist for the definition of a conceptual pore diameter, in this study a hydraulic diameter analogy is employed. The tortuosity, τ, of a porous medium is the ratio of the flow

path to the straight (line) path displacement of the particle. Permeability, a measure of hydraulic conductivity, is a property of the porous medium that depends upon the four characteristics mentioned above. Scheidegger [Ref. 10] presents methods used to measure the properties of porous media. Methods discussed are essentially experimental in nature.

The porous medium was modelled as shown in Figure 3.1. In Figure 3.1, D is the particle center-to-center distance, and d is the particle diameter. From the idealized geometry, the porosity for spherical particles is,

$$p = 1 - \frac{\pi}{6}\left(\frac{d}{D}\right)^3 \tag{3.1}$$

The pore diameter is obtained from an expression proposed by Carman [Ref. 11],

$$\delta = \frac{4p}{Z} \tag{3.2}$$

Equation 3.2 is analogous to a more familiar form of mean hydraulic diameter, 4v/A, where v is the void volume and A is the wetted surface area. The specific internal area, Z, based on the idealized geometry of Figure 3.1 may be expressed as,

$$Z = \frac{1}{2}\pi\frac{d^2}{D^3} \tag{3.3}$$

for spherical particles. Equation 3.3 is sometimes used and assumes one-half of the total internal surface area is effective for convective heat transfer. The fractional amount of total area is an estimate based on Fontenot's [Ref. 37] experimental results and does not generally apply to porous media [Ref. 9]. The Kozeny relations, alternate expressions of the specific internal area, are discussed by Scheidegger [Ref. 10]. Advantages of the Kozeny relations are fair agreement with experimental values and calculations that are independent of particle shape. A disadvantage is the failure of the relations to predict accurate values of Z at high values of porosity [Ref. 9]. For the geometric configuration of Figure 3.1, the tortuosity depends on the ratio d/D. Carman [Ref. 11] presents a table of measured tortuosity factors of various materials and geometries, and points out differences between analytical determinations of tortuosity. In this study, his recommended value of 1.4 is used. Particle size decreases with consumption. As a result, thermophysical properties which depend on particle diameter, as well as temperature, are functions of time and space. The numerical model presented assumes matrix rigidity as particle diameter decreases. This assumption gives rise to an increase in porosity during combustion. Although Scheidegger [Ref. 10] in his discussion of the packing theory of spheres, reports .875 porosity as the threshold for stability in a porous matrix, Carman [Ref. 11] reports on investigations performed on porosities as high

as 0.99. Changes in particle diameter are incorporated in the model and are discussed in Section III.D with carbon combustion.

B. DARCY'S LAW AND PORE VELOCITY

The Reynolds number for porous media is defined by

$$Re = \frac{\rho_a s d}{\mu} \tag{3.4}$$

where s is the local pore velocity, ρ is the mass density of air, and μ is the dynamic viscosity. The magnitude of the Reynolds number indicates whether fluid motion is dominated by molecular, viscous, or inertial effects. Most investigations of flow through porous media indicate flow regimes of viscous and inertially dominated flows. The Navier-Stokes equations apply to fluid motion possessing such Reynolds numbers. Because of the geometry involved in a consolidated (rigid) porous medium and the no-slip boundary condition (i.e., s = 0 at a solid-fluid interface), solution of the Navier-Stokes equations is difficult for a porous medium. Scheidegger [Ref. 10] points out that extensive experimental work with porous media indicates fluid flow is governed by Darcy's law for the range of Reynolds numbers where viscous effects dominate. The upper limit (velocity) Reynolds number in these investigations is subject to disagreement and varies from 0.1 to 75. Inertial effects

increase with increasing Reynolds numbers. Boffa [Ref. 12] has shown that for a fixed Reynolds number, inertial effects diminish with increasing air temperature. Darcy's law for two-dimensional flow is,

$$\hat{Q} = \frac{-m}{\mu} \cdot \left(\frac{dP}{dr}\hat{r} + \left(\frac{dP}{dz} - p\,\rho_a\, g\right)\hat{z}\right) \qquad (3.5)$$

where Q is the filter velocity or the volumetric flow rate per unit cross-sectional area; m is the specific permeability; g is the gravitational acceleration; $\hat{r}$ and $\hat{z}$ are the unit vectors in the r and z directions, respectively; and dP/dr and dP/dz are the pressure gradients in the r and z directions, respectively. The assumption here is that the r (radial) and z (axial) velocity components each react to the pressure independent of the other. The specific permeability of the porous medium used in the model is,

$$m = \frac{p}{96}\left(\frac{\delta}{\tau}\right)^2 \qquad (3.6)$$

Expression 3.6 is based on a cappilaric-serial model given by Scheidegger [Ref. 10]. Expressions for permeability vary with the physical assumptions of the flow paths incorporated into the model. Permeability also varies with the pore size distribution assumed. Physically, permeability and porosity are not related [Ref. 9]. Porosity is a quantifiable property of the porous medium, whereas permeability is a

constitutive property (i.e., a property specified by a constitutive relation, Darcy's law). The specific permeability is proportional to the filter velocity induced by a unit pressure gradient. Darcy's law is not derived from first principles but through exhaustive experimental analyses.

The Dupuit-Forcheimer assumption, addressed in Carman [Ref. 11], relates the local pore velocity to the filter velocity by,

$$\underset{\sim}{Q} = p \underset{\sim}{V} \quad , \tag{3.7}$$

The hypothesis is that the local pore velocity is greater than the filter velocity. The actual velocity in a single pore is a function of the fluid element's location within the pore. The Dupuit-Forcheimer assumption defines an "average" velocity within the pore.

The continuity equation for two-dimensional flow in porous media with nonconstant porosity distributions is,

$$\frac{D(p\rho_a)}{Dt} + p\,\rho_a \,\mathrm{Div}\,\vec{V} = 0 \tag{3.8}$$

Invoking the Dupuit-Forcheimer assumption and Darcy's law, the continuity equation becomes,

$$\frac{D(p\rho_a)}{Dt} + p\,\rho_a \,\mathrm{Div}\left[\frac{-m}{\mu\rho}\left(\frac{\partial P}{\partial r}\hat{r} + \left(\frac{\partial P}{\partial z} - p\,\rho_a\, g\right)\hat{z}\right)\right] = 0 \tag{3.9}$$

Equation 3.9 (neglecting body forces) is one of four field equations cast into a finite element formulation later in this work. From the pressure distribution, the pore velocity distribution is obtained by invoking Darcy's law and the Dupuit-Forcheimer assumption. The derivation of Equation 3.9 is presented in Appendix A.

C. SEMENOV MODEL OF COMBUSTION

The model of Semenov described in Frank-Kamenetskii [Ref. 13] and Vulis [Ref. 14], is the combustion model employed herein. The basis of the model is the relation of reaction rate to temperature and the interaction of heat generation and heat transfer. The reaction rate expression R_c, is the Arrhenius expression for a simple n-th order reaction,

$$R_c = A \phi^n \exp\left(\frac{-E}{R_u \hat{T}_c}\right) \tag{3.10}$$

where A is the time constant of the chemical reaction, E is the activation energy, R_u is the Universal Gas Constant, $\hat{T}_c$ is the absolute carbon temperature, and ϕ is the oxygen concentration. In a simple reaction, the reaction rate depends on the concentrations of reactants and not on the products. The heat generated by the reaction is obtained by multiplying Expression 3.10 by the heat (enthalpy) of combustion. As explained in [Ref. 13], a theory of combustion

can be constructed only if certain reasonable assumptions are made. For example, in order to regard the initial states as stationary, one must neglect the reaction rates at these states. The empirical law of chemical kinetics embodied in the Arrhenius expression tells us that the reaction rate never goes to zero but falls off exponentially with a decrease in temperature. Neglect of the reaction rate at the initial states is necessary to achieve initial equilibrium. In a finite range of temperatures above the initial states, neglect of reaction rates is also justifiable [Ref. 13]. At room temperature the reaction rates are on the order of 1.E-15 lbm-carbon/ft^2-hr or smaller, vice 1.E+3 lbm-carbon/ft^2-hr at 1500 °F.

D. ARRHENIUS LAW OF REACTION RATES

In 1934, Parker and Hottel [Ref. 15] proposed an Arrhenius expression for the reaction rate of carbon reacting in air. The expression assumed a simple first order reaction for the combustion of carbon in air. Frank-Kamenetskii [Ref. 13] has shown that the Parker and Hottel data is better correlated by a fractional order reaction, n between 1/3 and 2/3. A reaction order of 1/2 yields,

$$R_c = 2.065 \times 10^6 (R_{O_2} \phi)^{1/2} \exp(-57{,}240/R_u \hat{T}_c) \qquad (3.11)$$

In Expression 3.11, R_c is in units of lbm-carbon/ft^2-hr, R_{O_2} is the gas constant for oxygen (48.29 ft-lbf/lbm-R),

ϕ is in lbm/ft^3, R_u is 1.986 Btu/lbmole-R, and T_c is in Rankine. In order to determine the rate of heat generation and the rate of oxygen consumption, the chemical reaction for the combustion process must be considered. Although many complex chains in chemical kinetics generally describe combustion, a simple two-product analysis is employed in this formulation. For nonvolatile combustion of carbon and oxygen, two reactions that describe the process are,

$$C + \frac{1}{2} O_2 \rightarrow CO \tag{3.12}$$

$$C + O_2 \rightarrow CO_2 \tag{3.13}$$

where O denotes oxygen; and C, CO and CO_2 denote carbon, carbon monoxide and carbon dioxide, respectively. The ratio of the mass rates of carbon monoxide to carbon dioxide produced increases with increasing temperature. Arthur [Ref. 16] presents an expression for the rate ratio as a function of temperature (in Kelvin).

$$\frac{CO}{CO_2} = 2500 \exp(-6240/T_c) \tag{3.14}$$

The expression is valid for temperatures between 790 and 1170 K (1310-2110 degrees Fahrenheit). As a result of this temperature dependency, the stochiometric ratio and the heat of reaction are functions of temperature. Defining the fraction of carbon monoxide being produced by,

$$F_{CO} = (\frac{CO}{CO_2})/(1 + (\frac{CO}{CO_2})) \quad (3.15)$$

and the fraction of carbon dioxide as,

$$F_{CO_2} = 1/(1 + (\frac{CO}{CO_2})) \quad (3.16)$$

the heat of combustion is then expressed as,

$$\Delta H_R = F_{CO}\ \Delta H_{CO} + F_{CO_2}\ \Delta H_{CO_2} \quad (3.17)$$

Values for the heats of combustion, ΔH_{CO} and ΔH_{CO_2}, as functions of temperature may be obtained from JANAF (Joint Army, Navy, and Air Force) tables [Ref. 17]. For the range of temperatures being investigated (80-2000 degrees Fahrenheit), the heats of combustion are 3966.3 Btu/lbm for F_{CO} and 14,121. Btu/lbm for F_{CO_2}. Frank-Kamenetskii [Ref. 13] points out that over narrow ranges of temperature it is permissible to use an approximate expression which correctly describes the reaction rate. The stochiometric ratio (fuel to oxygen) of the overall reaction is,

$$f_R = f_{CO}\ f_{CO_2}/(f_{CO_2}\ F_{CO} + f_{CO}\ F_{CO_2}) \quad (3.18)$$

where f_{CO} is the stochiometric ratio for the reaction 3.12 and f_{CO_2} is the stochiometric ratio for the reaction 3.13. The rate of heat generation, R_g, and the rate of oxygen

consumption may now be expressed by,

$$R_g = \Delta H_R R_c \tag{3.19}$$

$$R_{O_2} = f_R^{-1} R_c \tag{3.20}$$

Parker's and Hottel's work [Ref. 15] and Arthur's work [Ref. 16] were conducted with specific types of carbon. Tables and references exist in Smoot and Pratt [Ref. 18] and Frank-Kamenetskii [Ref. 13] for rate expressions using other types of carbon. The present model allows for any simple fractional order rate expression of Arrhenius type to account for carbon consumption with CO and CO_2 byproducts. For this work the Parker and Hottel rate expression as modified by Frank-Kamenetskii (n = 1/2) is used.

Particle diameter decreases with progressive combustion. The rate of decrease depends on the amount of carbon consumed at a point over time. Observations have shown that the effect of decreasing particle diameter is significant when the reaction is concentrated in a small region of the porous medium. To account for this, an expression for the time rate of diameter change as a function of reaction rate is derived (Appendix B). For spherical particles the equation is,

$$\dot{d} = -2R_c Z D^3/(\pi \rho_c d^2) \tag{3.21}$$

where ρ_c is the bulk mass density of carbon. The diameter and the reaction rate are functions of time and space.

E. CARBON HEAT TRANSFER EQUATION FOR POROUS MEDIA

The heat transfer equations of the present investigation incorporate: (1) radiation (at boundaries where applicable), (2) internal convection, (3) conduction, (4) internal combustion, (5) temperature dependency of properties, and (6) compressibility effects of air into a two-dimensional (cylindrical coordinate) formulation. The carbon energy conservation equation is,

$$(1-p)\rho_c C_c \frac{\partial T_c}{\partial t} = \vec{\nabla}\cdot(1-p)(k_e)(\nabla T_c) - hZ(T_c-T_a) + R_g Z \qquad (3.22)$$

The derivation of Equation 3.22 is presented in Appendix A. The effective conductivity, k_e, of the porous solid was proposed by Russel [Ref. 24],

$$k_e = k_a \frac{p'^{2/3} + \frac{k_a}{k_c}(1 - p'^{2/3})}{p'^{2/3} - p' + \frac{k_a}{k_c}(1 - p'^{2/3} + p')} \qquad (3.23)$$

where k_c and k_a are bulk thermal conductivities of carbon and air respectively, and $p' = 1-p$. Russel's expression, which is based on an electrical analogy, is valid for the full range of porosities, 0.0 to 1.0.

Because of the difficulties encountered in a radiative analogy to Fourier's law of conduction, the particle to

particle radiative exchange in the porous medium is omitted. The difficulties are: (1) the geometry does not easily allow one to derive an expression for a "sink" temperature to use in a linearized approximation of the Stefan-Boltzman equation, and (2) the multi-wavelength characteristics of the radiation phenomenon are not easily incorporated.

F. HEAT TRANSFER EQUATION FOR AIR IN POROUS MEDIA

The internal convective heat transfer coefficient of Yoshida, Ramaswami, and Hougen [Ref. 33], is given by,

$$h = 0.91\ Re'^{-0.51}[\psi\ C_a\ G(C_a\mu/k_a)^{-2/3}]f_m \qquad (3.24)$$

where ψ is equal to 1 for spherical particles, G is a pseudo mass velocity given by $p\ \rho_a\ s$ and C_a is the specific heat of air at constant pressure. The f_m subscript indicates properties are to be evaluated at film temperature. Re' is a pseudo Reynolds number defined by,

$$Re' = G/z\ \mu\ \psi \qquad (3.25)$$

The air properties, as well as the internal convection coefficient, h, are temperature dependent. The reaction rate in Equation 3.22 is given by Expression 3.19.

An energy balance on the air within the porous medium obtains the second heat transfer equation,

$$p\rho_a C_a \frac{\partial T_a}{\partial t} = \vec{\nabla}\cdot(p\, k_a \nabla T_a) + hZ(T_c - T_a)$$

$$- p\,\rho_a C_a(\vec{V}\cdot\nabla)T_a - (\vec{V}\cdot\nabla)p\,P \qquad (3.26)$$

The density of air, ρ_a, is approximated by the ideal gas law. Pressure terms are due to the compressibility of air. The derivation of Equation 3.26 is presented in Appendix A. All properties in Equation 3.26 are temperature dependent. The properties of standard air were used in the model. Vatikiotis [Ref. 9] points out that tolerable differences (average of 7% difference) between standard air properties and properties accounting for the presence of byproducts CO and CO_2, is acceptable. Increased accuracy would introduce an additional mass balance equation for either CO or CO_2. Polynomial expressions used to calculate the thermophysical properties of air are those presented by Vatikiotis [Ref. 9]. The expressions are presented in Appendix B.

G. OXYGEN DIFFUSION EQUATION FOR POROUS MEDIA

The fourth field equation necessary to complete the system of equations is provided by an oxygen species conservation requirement. Transport mechanisms included in the model are molecular diffusion (Fick's law), convective mass flow and oxygen consumption due to combustion. Pressure and temperature induced concentration gradients are considered negligible. Vatikiotis [Ref. 9], provides examples for which

diffusion arising from pressure and temperature gradients is important. The oxygen mass balance equation is,

$$p \frac{\partial \phi}{\partial t} = \vec{\nabla} \cdot (p \mathcal{D}_e \nabla \phi) - \vec{\nabla} \cdot (p \phi \vec{V}) - R_{O_2} Z \qquad (3.27)$$

The derivation of Equation 3.27 is presented in Appendix A. The effective diffusivity, $\mathcal{D}_e$, proposed by Denbigh and Turner [Ref. 31] for a porous medium is

$$\mathcal{D}_e = \mathcal{D}/\tau \qquad (3.28)$$

Expression 3.28 accounts for the tortuosity encountered by the oxygen molecules as they flow through the porous medium. The semi-empirical expression proopsed by Gilliland [Ref. 34] is used to obtain the diffusivity of oxygen into air. The expression is,

$$\mathcal{D} = 435.7 \hat{T}_a^{3/2} (M_a^{-1} + M_{O_2}^{-1})^{1/2} / [P(V_a^{1/3} + V_{O_2}^{1/3})^2] \qquad (3.29)$$

where $\mathcal{D}$ is in units of cm^2/s, P is the total pressure in Pa, V_a and V_{O_2} are the molecular volumes of air and oxygen, respectively. M_a and M_{O_2} are the molecular weights of air and oxygen. The values of V_a and V_{O_2} may be obtained in Holman [Ref. 35] as 29.9 and 7.4 cm^3, respectively. The oxygen consumption term in Equation 3.27 is given by Expression 3.20.

H. BOUNDARY CONDITIONS

Boundary conditions employed were as follows for the carbon,

$$\left.\frac{\partial T_c}{\partial r}\right|_{\frac{r}{r_o}=0} = 0 \tag{3.30}$$

$$(1-p)(k_e)\left.\frac{\partial T}{\partial z}\right|_{\frac{z}{z_o}=0} = -q''_s \tag{3.31}$$

where q_s is the starting heat flux.

$$(1-p)(k_e)\left.\frac{\partial T}{\partial z}\right|_{\frac{z}{z_o}=1} = -\sigma\varepsilon(\hat{T}_c^4 - \hat{T}_\infty^4) \tag{3.32}$$

$$(1-p)(k_e)\left.\frac{\partial T}{\partial r}\right|_{\frac{r}{r_o}=1} = \begin{cases} 0 & \text{(1-D problems)} \\ h_r(T_c-T_\infty) + \sigma\varepsilon(\hat{T}_c^4-\hat{T}_\infty^4) & \text{(2-D problems)} \end{cases} \tag{3.33}$$

For air,

$$\left.\frac{\partial T_a}{\partial r}\right|_{\frac{r}{r_o}=0} = 0 \tag{3.34}$$

$$p\,k_a\left.\frac{\partial T_a}{\partial z}\right|_{\frac{z}{z_o}=0} = p\,\rho_a C_a v(T - T_\infty) \tag{3.35}$$

$$T_a\Big|_{\frac{z}{z_o}=0} = T_\infty \tag{3.35a}$$

$$p\,k_a \frac{\partial T_a}{\partial z}\Big|_{\frac{z}{z_o}=1} = -\,p\,\rho_a C_a\, v(T_a - T_\infty) \tag{3.36}$$

$$p\,k_a \frac{\partial T_a}{\partial r}\Big|_{\frac{r}{r_o}=1} = \begin{cases} 0 & \text{(1-D problems)} \\ h_r(T_a - T_\infty) + \sigma\varepsilon(\hat{T}_a^4 - \hat{T}_\infty^4) & \text{(2-D problems)} \end{cases} \tag{3.37}$$

For pressure,

$$\frac{\partial P}{\partial r}\Big|_{\frac{r}{r_o}=0} = 0 \tag{3.38}$$

$$P\Big|_{\frac{z}{z_o}=0} = P_1 \tag{3.39}$$

$$P\Big|_{\frac{z}{z_o}=1} = P_2 \tag{3.40}$$

$$\frac{\partial P}{\partial r}\Big|_{\frac{r}{r_o}=1} = 0 \tag{3.41}$$

Finally, for O_2 concentration,

$$\left.\frac{\partial \phi}{\partial r}\right|_{\frac{r}{r_o}=0} = 0 \tag{3.42}$$

$$p\,\mathcal{D}_e \left.\frac{\partial \phi}{\partial z}\right|_{\frac{z}{z_o}=0} = v(\phi - \phi_\infty) \tag{3.43}$$

$$\left.\phi\right|_{\frac{z}{z_o}=0} = \phi_\infty \tag{3.43a}$$

$$p\,\mathcal{D}_e \left.\frac{\partial \phi}{\partial z}\right|_{\frac{z}{z_o}=1} = v(\phi - \phi_\infty) \tag{3.44}$$

$$p\,\mathcal{D}_e \left.\frac{\partial \phi}{\partial r}\right|_{\frac{r}{r_o}=1} = 0 \tag{3.45}$$

Equations 3.35, 3.36, 3.43, and 3.44 correspond to convective flux conditions on air temperature and O_2 concentration. At the air inlet ($\frac{r}{r_o} = 0.0$), Dirichlet conditions, Equations 3.35a and 3.43a may be imposed on the air temperature and oxygen concentration. The idea behind this treatment is that in the presence of a semi-infinite medium (ambient air), the air and O_2 concentration may be considered, to a first approximation, very near ambient conditions. Equations 3.30, 3.34, 3.38 and 3.42 correspond to symmetry conditions at

$\frac{r}{r_o} = 0.0$. Equations 3.33, 3.37, 3.41 and 3.45 correspond to impermeable boundaries and insulated boundaries at $\frac{r}{r_o} = 1.0$ and are used in conjunction with one-dimensional problems. The second part of Equations 3.33 and 3.37 are the boundary conditions that represent a relaxation of the radial insulation of carbon and air temperatures which allow the system to become a two-dimensional heat transfer problem. It must be pointed out however that the heat transfer coefficients of Equations 3.33 and 3.37 are not easily obtained. This work could not proceed if the following assumptions were not made. It was assumed that the air and carbon had near equal profiles at $\frac{r}{r_o} = 1.0$ so that the same heat transfer coefficient would apply to both variables. If Equation 3.35 is used as a boundary condition, the air temperature follows closely the carbon temperature at $\frac{r}{r_o} = 1.0$. Furthermore it was assumed for simplicity of calculation that the heat transfer coefficient was constant. The difficulty is as follows. In order to determine the heat transfer coefficient for the impressed temperature profiles at $\frac{r}{r_o} = 1.0$, the temperatures themselves must be known. The correct procedure would involve an initial estimate of the profile, calculation of the heat transfer coefficient, solution of the problem for one integration and verification of the assumed and calculated temperature profiles. Upon suitable verification of the profiles, the same procedure is performed for the next integration. Other problems arise for example if the radial heat transfer at

$\frac{r}{r_o}$ = 1.0 is of natural convective type. At the exit $\frac{z}{z_o}$ = 1.0, functional and derivative continuity must be demonstrated for pressure, oxygen concentration and air temperature at the vertical boundary separating the stream of exiting air and the convective boundary layer. This is known as a conjugate problem. The above method is a realistic method for the treatment of this problem but admittedly it is beyond the scope of this work. The numerical code has provisions for incorporating an average of isoflux and isothermal natural convective Nusselt number formulations (Churchill correlations) for vertical cylinders obtained from [Ref. 36]. Although the subroutine has been written there has been no attempt to date to implement it. It is known that physically heat transfer coefficients lie between those generated from isothermal and isoflux considerations. However, simply having empirical correlations for evaluating the heat transfer coefficients does not eliminate the need of the iterative scheme described above. Additional considerations must be addressed in this context. In order to effect an impermeable vertical boundary at $\frac{r}{r_o}$ = 1.0, the system must be enveloped by a cylindrical container fabricated of some type of material. This material has an inherent potential to absorb internal energy that transits from the initial system to the boundary where some flowing medium is able to convect energy away (Figure 3.2). The material's ability to absorb energy adds a thermal resistance to the heat transmission in an electical

analog sense (Figure 3.3) and thus affects the temperature profile and ultimately the heat transfer coefficients. Of necessity then, the material's inherent ability to absorb energy is denied. No attempt is made here to conjecture as to how physically one may impose the radial boundary conditions implemented below. If it were possible to rigorously apply the heat transfer boundary condition described above, the numerical model would be capable of obtaining a solution. The model was tested at various values of constant heat transfer coefficient: 0, 1, 5, 50, 100, 500, to determine the effect of the heat transfer coefficient on the solution. It was found that until the heat transfer coefficient gets significantly large compared to the start flux applied to the carbon at the air inlet boundary (in this case above 100 Btu/ft^2-hr compared to 1500 flux applied to carbon), the two-dimensional effects on the temperature profile were localized in the $\frac{r}{r_o}$ = 0.85 to 1.0 region. The temperature profiles for $\frac{r}{r_o}$ less than 0.85 were essentially one-dimensional (constant value independent of r).

I. INITIAL CONDITIONS

The model is developed so each problem begins at a uniform initial temperature. A heat flux applied to the carbon along a boundary provides a means of bringing the system to a temperature level where reaction terms are sufficiently high to generate combustion. The heat flux is treated as follows,

$$(1-p)\nabla(k_e)\frac{\partial T_c}{\partial z}\Big|_{\frac{z}{z_o}=0} = -q''_s \qquad (3.46)$$

Expression 3.46 is incorporated into the numerical formulation as Neumann boundary condition for carbon temperature. The initial heat flux may be turned off at any specified time. The boundary condition of Expression 3.46 then switches to a Cauchy (mixed) boundary condition to account for radiative heat transfer from the carbon particles at the boundary to the ambient air. Convective heat transfer from the carbon particles to the air is treated through the internal heat transfer coefficient. The above procedures for treating problem initiation obviate the need of trying to specify initial conditions which may in general be arbitrary for each problem.

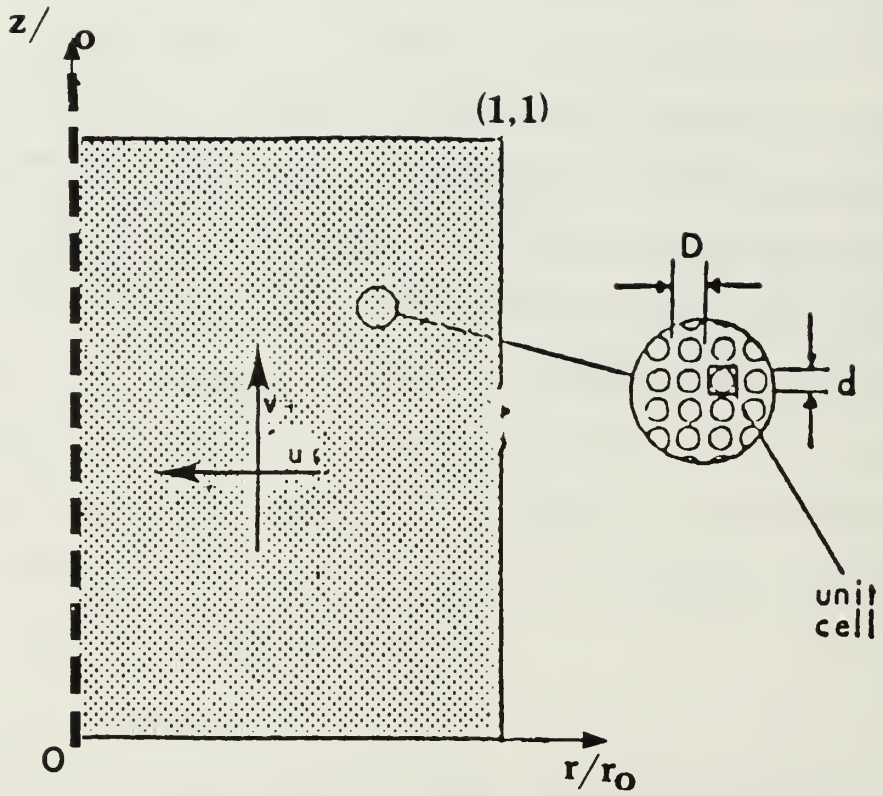

Figure 3.1 Geometric Model of Porous Medium

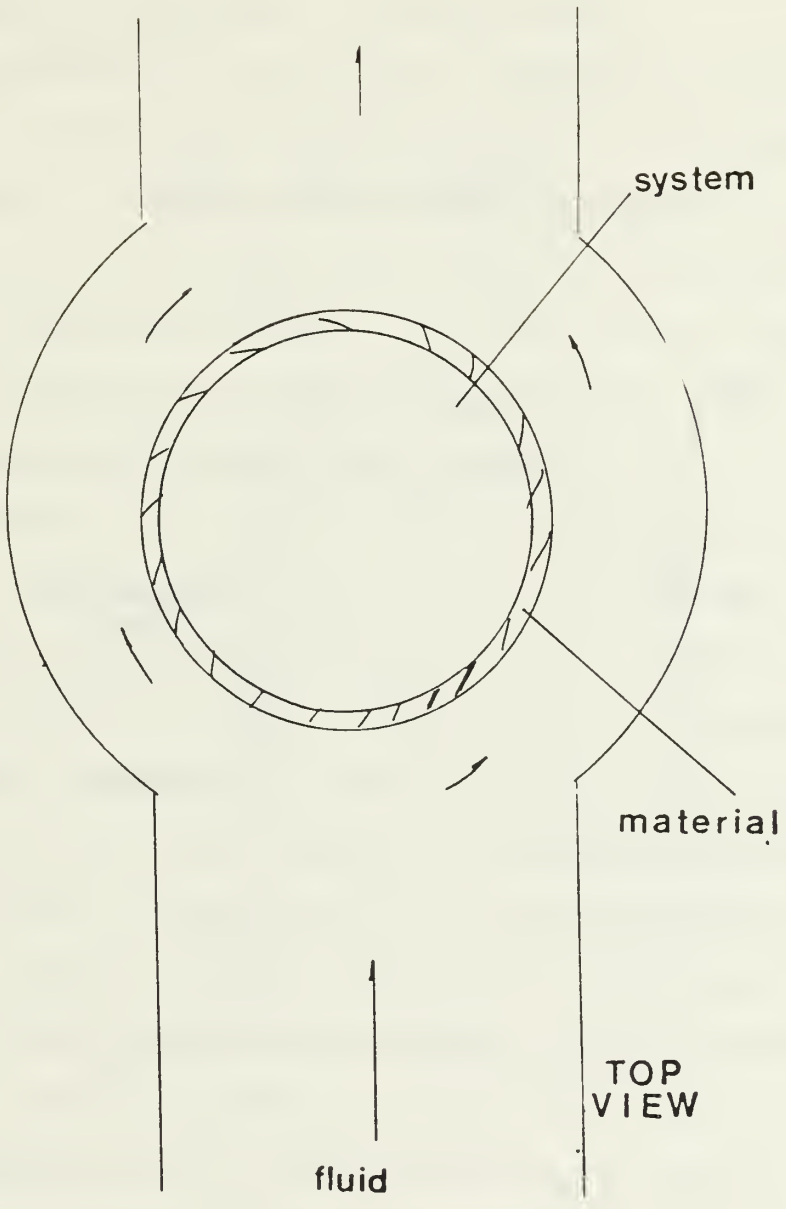

Figure 3.2 Top View of Radial Convection Circuit

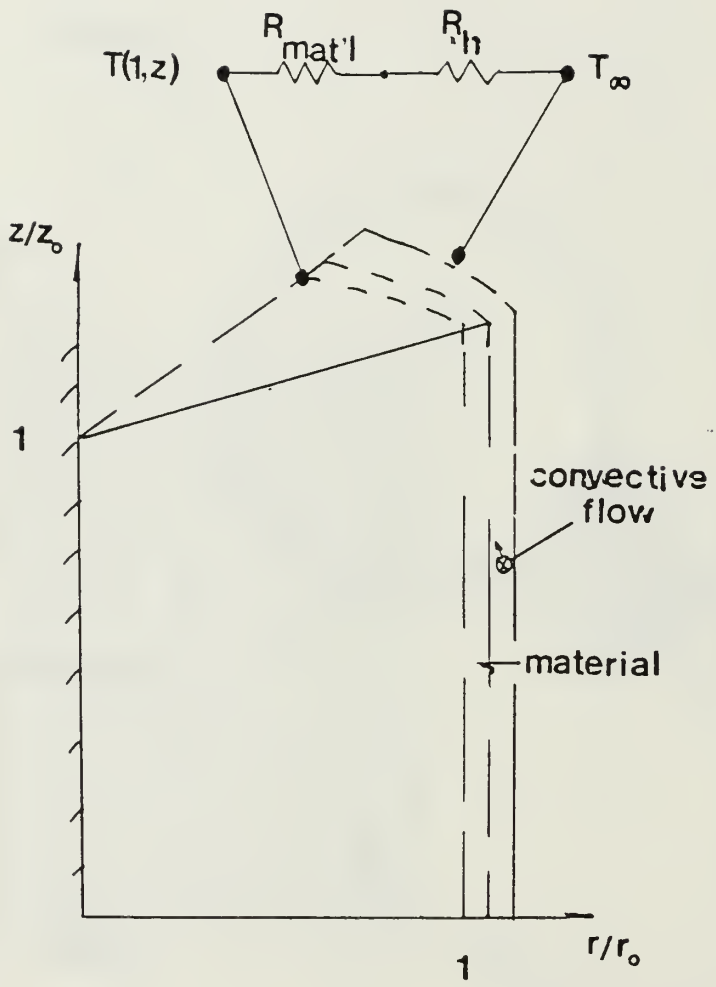

Figure 3.3 Electrical Analogy of Thermal Circuit at $r/r_o = 1.0$

IV. NUMERICAL CONSIDERATIONS

A. TREATMENT OF NONLINEAR COMBUSTION TERM

The treatment of the nonlinear combustion term is now discussed in brief detail highlighting the advantages of each treatment. A more comprehensive discussion is presented in Appendix C. The interested reader is encouraged to review the detailed analysis. There are several ways to treat the Arrhenius reaction rate expression.

1. Excitation (Force) Term Treatment

Perhaps the simplest method for incorporating the combustion term is to evaluate it at each time step and use the evaluated value (held constant) as an estimate of the mean value during the next integration. It is realized that in fact, the value is not constant in real time. This treatment, however, provides a means of incorporating the term into the system of equations as a first approximation with relatively little computational effort. Averaging techniques exist for improving upon this method. In this scheme the excitation vector is modified at each nodal point in the carbon temperature and oxygen concentration equations to include the combustion terms. The exponential reaction rate term that appears in both the porous solid and oxygen diffusion equation is,

$$R_c = A \phi^n \exp(-E/R\hat{T}_c) \qquad (4.1)$$

In the carbon equation, Expression 4.1 appears as,

$$R_g = \Delta H_R \cdot R_c \tag{4.2}$$

In the oxygen concentration equation, Expression 4.1 appears as,

$$R_{O_2} = f_R^{-1} \cdot R_c \tag{4.3}$$

The term that is to be evaluated at the last time step and to be held constant over the next time step is,

$$R_c = \{A \phi^n \exp(-E/R\hat{T}_c)\}^{*t_{n-1}} \tag{4.4}$$

where the superscript $*t_{n-1}$ indicates evaluation occurring at the previous time step.

2. Linear Operator Treatment of O_2 Concentration

In order to realize an improvement over the first treatment one may retain a portion of the reaction expression as an operator by making the following rearrangement:

$$R_c = \{A \phi^{n-1} \exp(-E/R\hat{T}_c)\}^{*t_{n-1}} \cdot [\phi] \tag{4.5}$$

where $[\phi]$ denotes a spatial operator treatment of the response variable.

3. Bilinear Operator Treatment of O_2 and T_c

The bilinear operator treatment of the reaction rate is the present method of treatment. The reaction rate term is rearranged as follows,

$$R_c = \left\{\frac{A\,\phi^{n-1}\exp(-E/R\hat{T}_c)}{T_c}\right\} {}^{*}t_{n-1} \cdot [T_c\phi] \qquad (4.6)$$

Letting

$$T_c = \xi_i^T \theta_{1i} , \quad i = 1,3 \qquad (4.7)$$

and

$$\phi = \xi_i^T \theta_{4i} , \quad i = 1,3 \qquad (4.8)$$

and invoking natural coordinates [Ref. 28], an elementally averaged contribution results in the following area integral,

$$\underset{\approx}{C} = \bar{C} \int_{A_e}\int \underset{\sim}{\xi}\,\underset{\sim}{\xi}^T \underset{\sim}{\theta}_1\,\underset{\sim}{\xi}^T \underset{\sim}{\theta}_4 \, dA \qquad (4.9)$$

The double subscript permutation of carbon temperature and O_2 concentration results in a 3×9 elemental matrix that is distributed into the system equations. In this scheme at each nodal point within an element, carbon temperature and O_2 concentration equations receive nine terms arising from

combustion occurring within the element. An element loop is performed to account for combustion terms in an elementally averaged sense over the entire system spatial domain.

B. OPTIMAL COMPACT STORAGE (OCS)

The optimal compact storage scheme, presented by Franke and Salinas [Ref. 29], employed in the solution of the combustion problem, allowed the computational effort to proceed with substantial savings in computer storage, computer-run time, and ultimately dollar cost per run. In the optimal compact storage scheme, only the non-zero coefficients are stored in a vector array. This results in a very significant reduction of the storage area compared to banded storage. One might encounter problems on the order of 1000×1000 DOF. (In this problem there are four degrees of freedom at each nodal point. A 17×17 grid requires a 1156×1156 matrix if full storage is employed.) For banded storage the bandwidth might be 200. The storage ratio for bandwidth to full storage would be 0.2. Using OCS, a conservative estimate of the average number of equation entries in this model is 20. The ratio of OCS to banded storage is 0.1. Thus in this example, the savings realized by OCS vice full storage is 98%!

C. GRID CONVERGENCE

A convergence study was done on the response field for several grids. It was found that non-uniform grids were far

superior to uniform grids. In fact, for many problems, computer storage limitations require that a non-uniform grid be used to obtain reasonably accurate solutions. Non-uniform grids allow the investigator to take advantage of the knowledge of areas of severe combustion induced gradients. "Stacking" elements in these areas assists the algorithm in producing more accurate and numerically stable results. For similar degrees of accuracy with uniform grids, it is estimated that grids on the order of 1000 × 1000 nodal points (and larger) would have been required. Nondimensionalized length discretizations on the order of .001-.005 and smaller near the air inlet boundary permit excitations on the system boundaries to be propagated accurately through the medium. Until discretizations on the order of non-dimensionalized lengths of 0.001 were employed, numerical instability was encountered in the carbon temperature field. This instability was manifested by severe overshoot, leading to negative temperatures in close proximity to severe thermal gradients.

For non-uniform grids it was found that grids below 10 nodal points in each direction were not adequate. The temperatures obtained from these models were lower due to the relatively low degree of grid refinement or discretization possible with such few points. Grid refinement in this type of problem is essential to capture the high activity (large gradients) that is inherent in the combustion phenomenon.

A convergence study was done on several nodal points at various times for non-uniform grids at 12 × 12, 17 × 17, and

22 × 22 nodal points. The solution changed 5% from a 12 × 12 to a 22 × 22 nodal point model. Next, a 17 × 17 point non-uniform grid model was investigated. It was found that the solution changed approximately 2% from the 22 × 22 nodal point model. At this point, it was determined that the 12 × 12 non-uniform nodal point afforded the desired balance between cost, computational effort and computer-run time.

grid size (n × n)	kmax	clock runtime (min.)
12	6,398	70
17	13,223	100
22	22,498	110

D. MODEL VALIDATION TESTS

In order to validate the capabilities and accuracy of the numerical code, several tests were conducted.

1. The Steady State Problem

First, it was necessary to ensure the model's ability to recognize a steady state condition. This was the simplest of all tests (and first to be) performed. Initial (ambient) conditions were imposed uniformly throughout the system on the four fields: carbon temperature and air temperature (80 degrees F.), pressure (2,116.8 psf) and oxygen concentration (0.0172 lbm/ft^3). An initial integration time step equal to the minimum time step allowable (user input) 1.E-6 hr., was selected. In less than five integrations the algorithm switched to the maximum allowable time step (user input)

5.E-1 hr., and iterated about the given initial fields. This sufficiently demonstrated the first of several tests requisite to assure numerical code compatibility with the integration scheme.

2. The Finite Slab

Consider the slab of thickness 2L in Figure 4.1(a). One seeks the solution of the one-dimensional conduction equation,

$$\frac{\partial T}{\partial x} = \alpha \frac{\partial^2 T}{\partial x^2} \tag{4.10}$$

subject to an initial condition,

$$T(x,0) = T_i \tag{4.11}$$

and uniform convection conditions at both surfaces: At $x = \pm L$:

$$-k \frac{\partial T}{\partial x} = \pm h(T - T_o) \tag{4.12}$$

The exact solution is given as a Fourier series in [Ref. 23],

$$\theta = \frac{T - T_o}{T_i - T_o} = \sum_{i=1}^{\infty} C_i \, e^{-\beta^2 \alpha t / L^2} \cos(\beta_i \frac{x}{L}) \tag{4.13}$$

where,

$$C_i = \frac{4 \sin \beta_i}{2\beta_i + \sin(2\beta_i)} \tag{4.14}$$

The constants β_i are the roots of the transcendental algebraic equation,

$$\beta_i \tan \beta_i = B_i = h_o L/k \tag{4.15}$$

Thus the solutions have the Biot number of the slab as a parameter. The roots of Equation 4.15 are tabulated in Appendix A to [Ref. 25].

3. The Cylinder

Consider the cylinder of Figure 4.1(b). The suddenly immersed cylinder satisfies the equation,

$$\frac{\partial T}{\partial t} = \frac{\alpha}{r} \frac{\partial}{\partial r}(r \frac{\partial T}{\partial r}) \tag{4.16}$$

subject to an initial condition,

$$T(r,0) = T_i \tag{4.17}$$

and a convection condition at the surface: At $r = r_o$,

$$-k \frac{\partial T}{\partial r} = h_o (T - T_o) \tag{4.18}$$

The solution is given as a Fourier series in [Ref. 23]:

$$\theta = \frac{T - T_o}{T_i - T_o} = \sum_{i=1}^{\infty} C_i e^{-\beta_i^2 \alpha t / r_o^2} J_o(\beta_i r / r_o) \qquad (4.19)$$

where,

$$C_i = \frac{2}{\beta_i} \frac{J_1(\beta_i)}{J_o^2(\beta_i) + J_1^2(\beta_i)} \qquad (4.20)$$

The constants β_i are the roots of the algebriac equation,

$$\beta_i J_1(\beta_i)/J_o(\beta_i) = B_i = h_o r_o / k \qquad (4.21)$$

The functions J_o and J_1 are the Bessel functions of the first kind whose numerical values are tabulated in most advanced engineering mathematics texts. For a limited range of interest, numerical values of J_o and J_1 are tabulated in Appendix A of [Ref. 25]. The roots of Equation 4.21 are tabulated in [Ref. 23].

4. Multidimensional Solutions by the Product Method

The classic solutions for semi-infinite- and finite-thickness bodies (slabs, cylinders and spheres) may be used to generate solutions for multidimensional bodies.

Use of the product solution technique is illustrated by Figure 4.2. The problem chosen to validate the heat transfer portion of the current model is the "sudden immersion" problem for a finite-length cylinder subjected to

uniform convection conditions (h_o, T_∞) on all sides and initial uniform temperature T_i. The differential equation to be solved is,

$$\frac{1}{r}\frac{\partial}{\partial r}\left(r\frac{\partial\theta}{\partial r}\right) + \frac{\partial^2\theta}{\partial x^2} = \frac{1}{\alpha}\frac{\partial\theta}{\partial t} \tag{4.22}$$

where $\theta = (T - T_o)/(T_i - T_o)$. The initial condition is

$$\theta(r,x,0) = 1 \tag{4.23}$$

The convection boundary conditions are,

At top and bottom:
$$-k\frac{\partial\theta}{\partial x} = \pm h_o\theta \tag{4.24}$$

On the sides:
$$-k\frac{\partial\theta}{\partial r} = h_o\theta \tag{4.25}$$

The solution is the product of the two simpler analyses: the semi-infinite slab and the infinite cylinder. Let

$$\theta(x,r,t) = \theta_{slab}(x,t) \cdot \theta_{cyl}(r,t) \tag{4.26}$$

$$= P(x,t) \cdot C(r,t)$$

Substituting Equation 4.26 into Equations 4.22, 4.23 and 4.24 and separating the variables, reduces the two-dimensional problem into two one-dimensional problems:

Slab: $$\frac{\partial^2 \theta_s}{\partial x^2} = \frac{1}{\alpha}\frac{\partial \theta_s}{\partial t} \qquad (\theta_s = \theta_{slab})$$

$$\theta_s(x,0) = 1$$

$$-k \left.\frac{\partial \theta_s}{\partial x}\right|_{x = \pm L} = h_o \theta_s(\pm L, t)$$

Cylinder: $$\frac{1}{r}\frac{\partial}{\partial r}\left(r \frac{\partial \theta_c}{\partial r}\right) = \frac{1}{\alpha}\frac{\partial \theta_c}{\partial t} \qquad (\theta_c = \theta_{cyl})$$

$$\theta_c(r,0) = 1$$

$$-k \left.\frac{\partial \theta_c}{\partial r}\right|_{r_o} = h_o \theta_c(r_o, t)$$

Thus Equation 4.26 is the exact solution to the sudden immersion problem of a right circular cylinder.

5. Validation Problem

The validation problem is Example 4.9 in [Ref. 25]. The problem is stated here for the convenience of the reader.

The short cylinder in Figure 4.3 is initially at 40° C and then plunged into a fluid with h = 300 W/m-K and T = 200° C. The material is bronze, k = 26 W/m-K and $\alpha = 8.6 \cdot 10^{-9}$ m^2/s. Find the temperature at the center of the cylinder after 5 minutes.

Solution: 176° C (348.8° F). The details of the solution are found on pages 186-187 of [Ref. 25]. The product solution technique was utilized in obtaining a 5-term approximation of the series solution for Fourier moduli ($F_o = \alpha t/L^2$, equivalent to a nondimensionalized time) less than 0.2. For Fourier moduli greater than 0.2, a two-term approximation of the exact solution was used. Heisler [Ref. 26] points out that a one-term approximation of the exact series solution yields an accuracy to within 1% of the exact value for Fourier moduli greater than 0.2. Various values (5, 10, 20 and 30 seconds) corresponding to values of Fourier moduli less than 0.2 were used in comparing model solutions with the exact (five-term approximations to the exact) solution. Values (3, 5, 7 and 9 minutes) corresponding to Fourier moduli greater than 0.2 were used to compare model solutions with the exact (one-term approximations with 1% accuracy) solutions. Figures 4.4 through 4.8 show: (1) the effects of time on the solution of various grids, and (2) effects of grid refinement at equal values of time. Values plotted on the ordinate scales are deviation (percentage error) from the exact solutions versus time. Observation yields that for small values of time, grid refinement obtains more accurate results and obtains a faster convergence to steady state.

6. Testing the Model's Ability to Accept and Reject Heat

An equivalent simple test in model validation is the model's ability to accept heat from a boundary flux and

reject it at a later time to its environment via convection. The applied heat flux at $\frac{z}{z_o} = 0$ is 1500 Btu/ft^2-hr. Figures 4.9-4.12 illustrate system response. Figure 4.13 is the input data set used.

7. The One-Dimensional Problem

Another step in the validation of the two-dimensional problem is an examination of a one-dimensional problem. One might infer that a two-dimensional model includes the one-dimensional model as a subset. This was demonstrated in a separate test. A one-dimensional problem may be imposed on the model in two ways. One way is to make the length to diameter ratio very large. (No restrictions on excitations is implied.)

Another method for eliciting one-dimensional behavior is to "excite the system in a one-dimensional fashion," i.e., apply boundary conditions at $\frac{z}{z_o} = 0.0$ and $\frac{z}{z_o} = 1.0$ independent of radius and insulate radial boundaries at $\frac{r}{r_o} = 0.0$ and $\frac{r}{r_o} = 1.0$. The insulated boundary at $\frac{r}{r_o} = 0.0$ arises from an axisymmetric formulation of the problem. The zero gradient (completely insulated) boundary at $\frac{r}{r_o} = 1.0$ corresponds to a completely (all four variables) impermeable vertical boundary. For this problem, an adiabatic restriction is sufficient. In general, an adiabatic condition means an insulation of heat. In this problem, the implication is far greater because of the coupling between system fields. An adiabatic restriction at $\frac{r}{r_o} = 1.0$ prohibits non-zero radial

pressure gradients. Unconstrained radial pressure gradients at $\frac{r}{r_o} = 1.0$ imply radial convection of air enthalpy and in a non-isothermal fluid, this convection undermines the initial adiabatic assumption at $\frac{r}{r_o} = 1.0$. Oxygen gradients are also negated by an adiabatic condition since oxygen convection by air must occur under the presence of nonzero pressure gradients at $\frac{r}{r_o} = 1.0$.

The two methods described above distinguish one-dimensional behavior arising from geometrical conditions and one-dimensional behavior resulting from restrictions on excitations. Figures 4.14-4.16 depict model one-dimensional solutions to "one dimensional excitations." Figure 4.17 is the input data set used.

Figure 4.1 Classical Transient 1-D Geometries

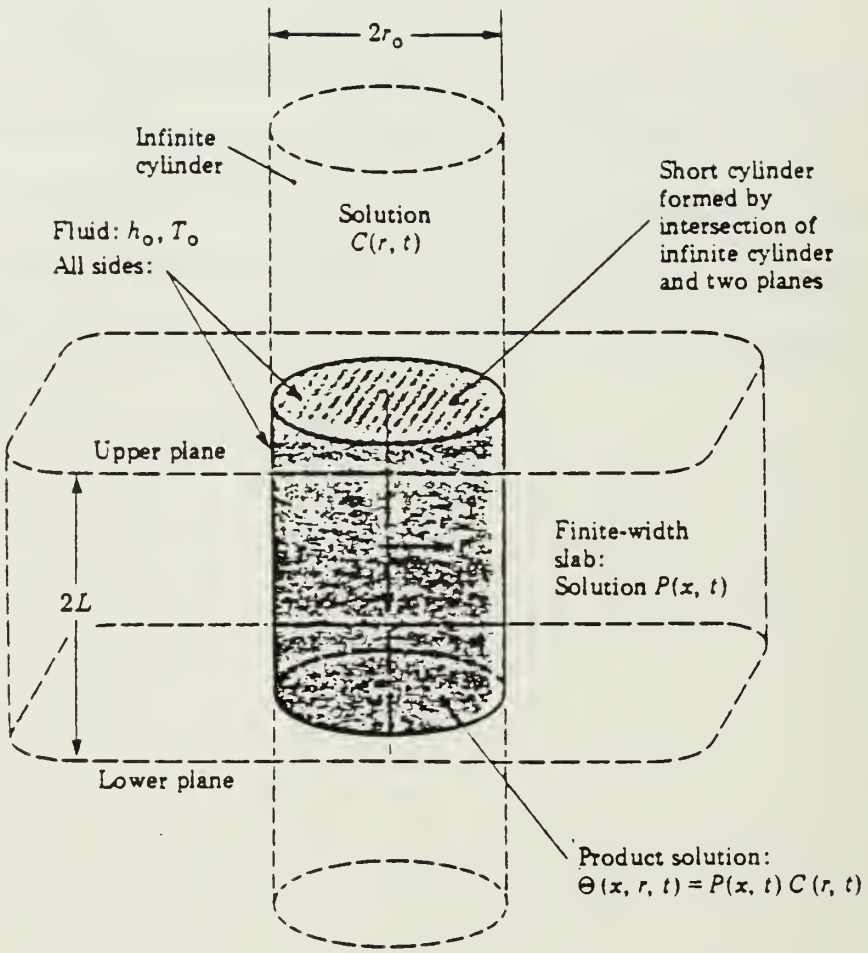

Figure 4.2 Illustration of the Product Technique

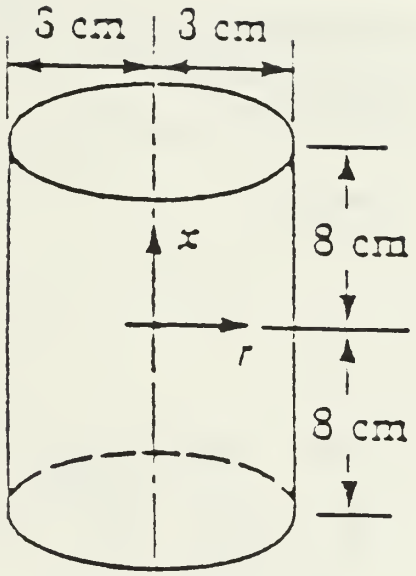

Figure 4.3 Sample Problem, Cylinder Geometry

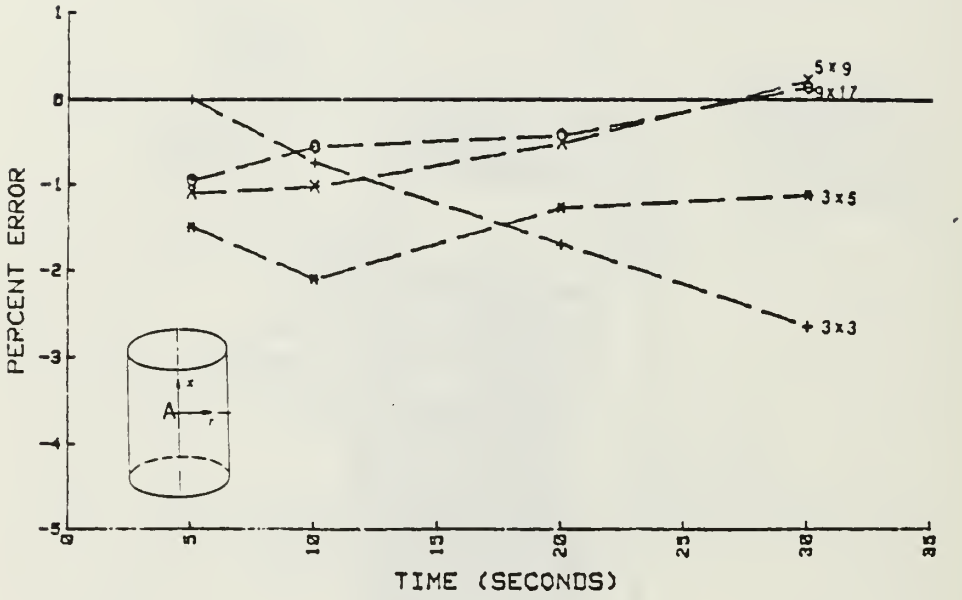

Figure 4.4 Grid Effects at Point A, (0,0)

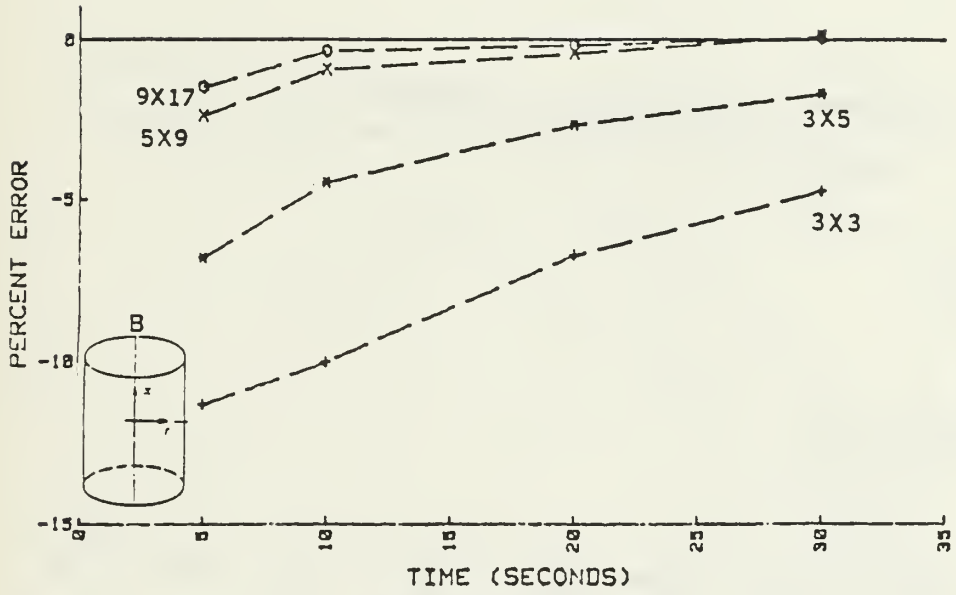

Figure 4.5 Grid Effects at Point B, (0,1)

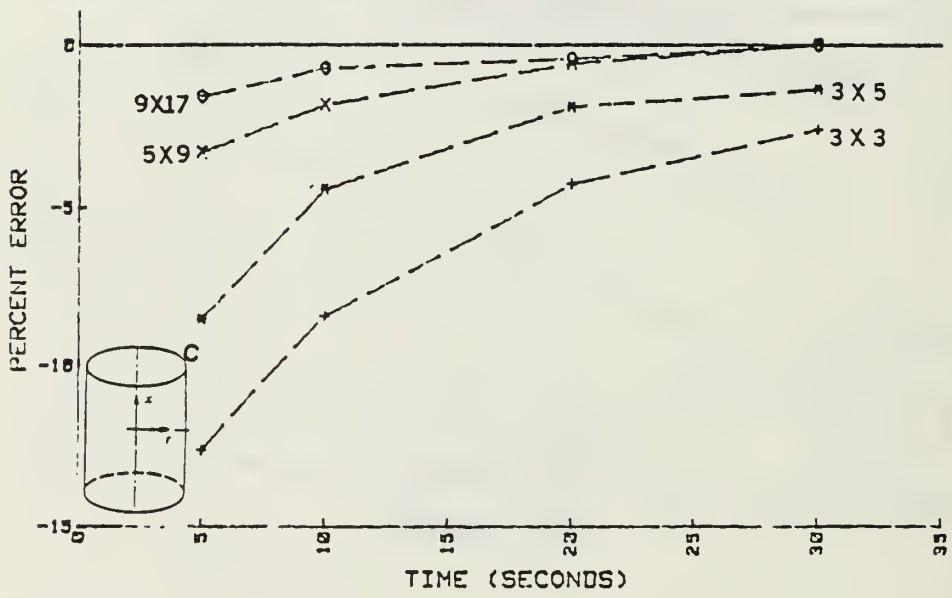

Figure 4.6 Grid Effects at Point C, (1,1)

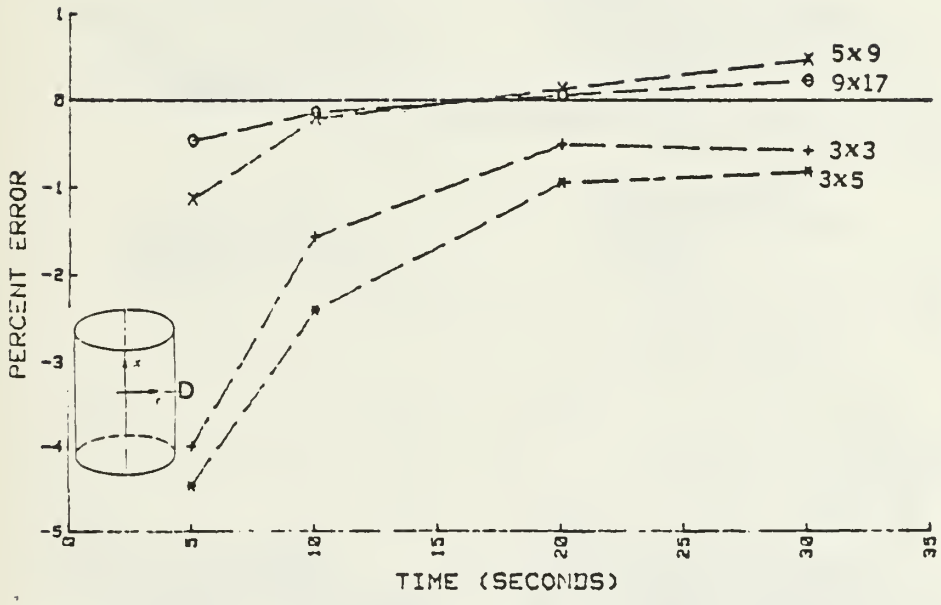

Figure 4.7 Grid Effects at Point D, (1,0)

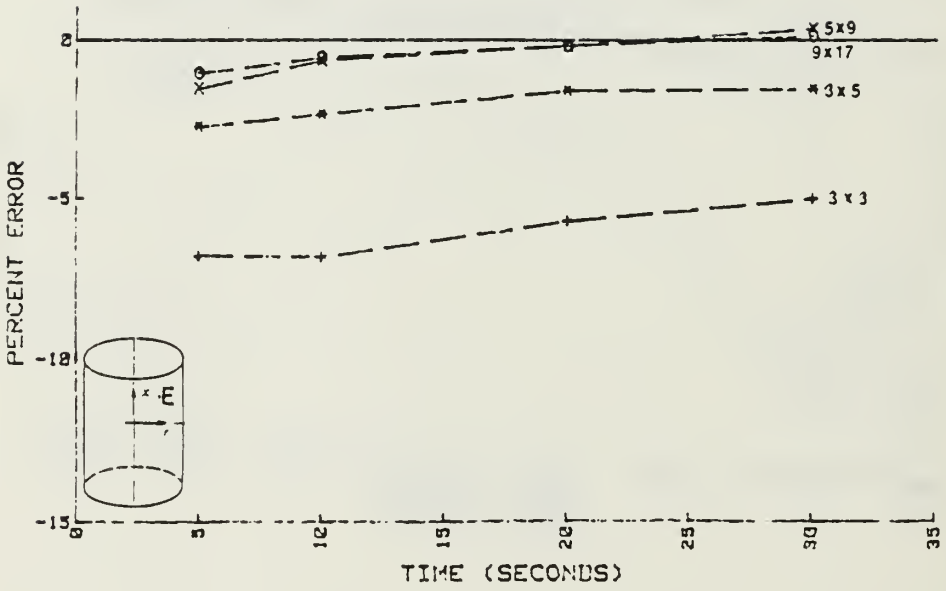

Figure 4.8 Grid Effects at Point E, (.5,.5)

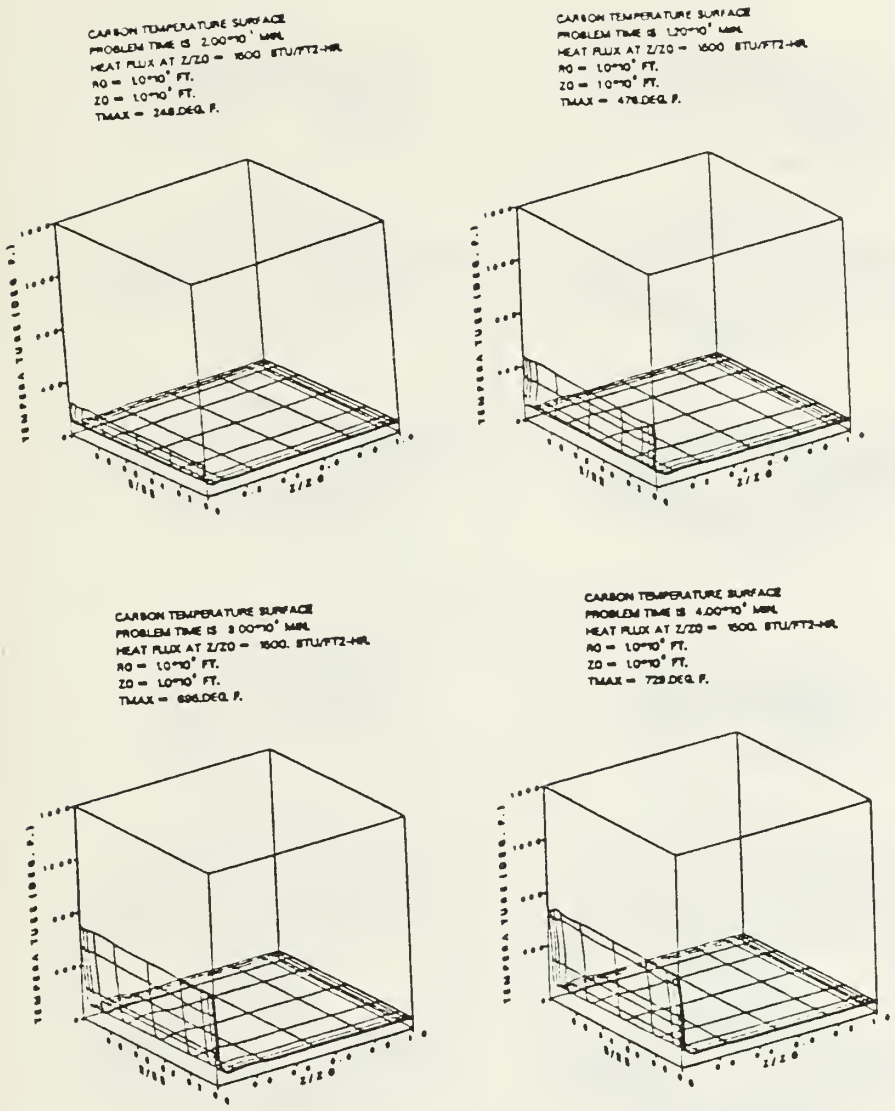

Figure 4.9 Model Accepting Heat (Carbon Temperature Profile)

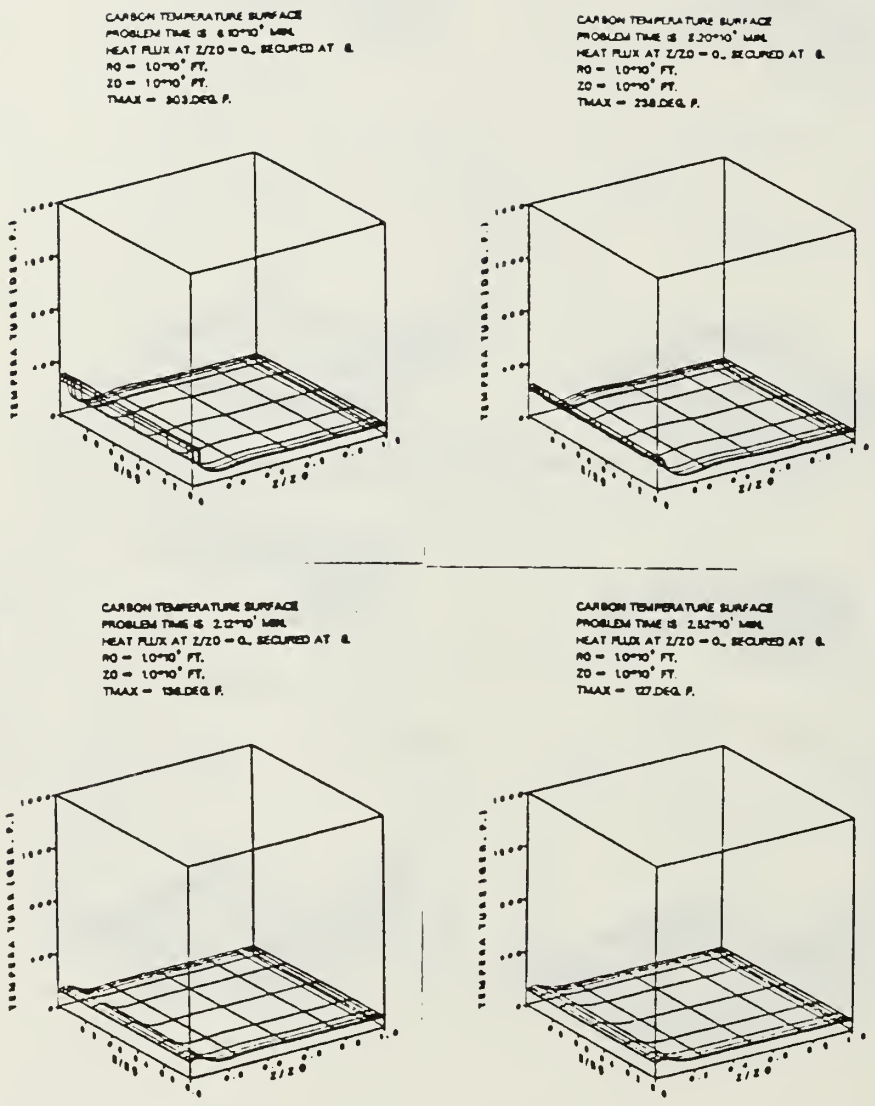

Figure 4.10 Model Rejecting Heat (Carbon Temperature Profile)

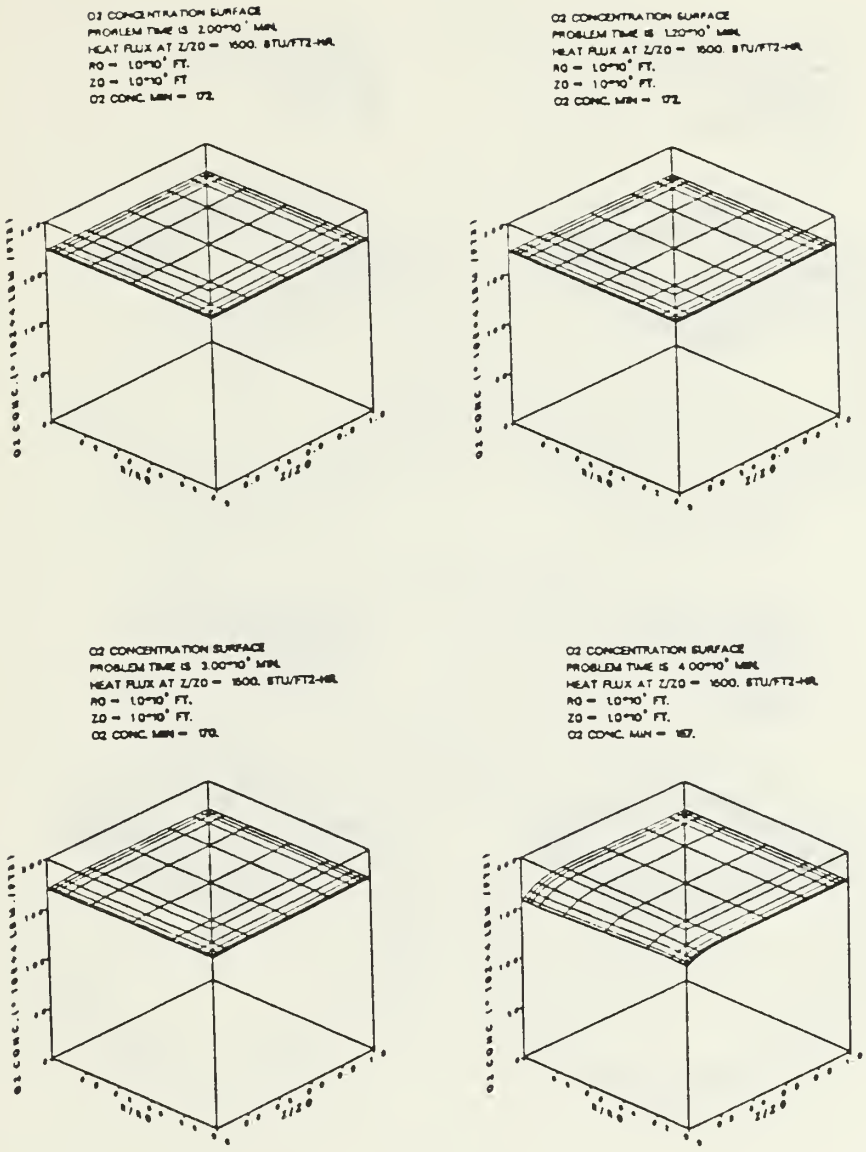

Figure 4.11 Model Accepting Heat (Oxygen Concentration Profile)

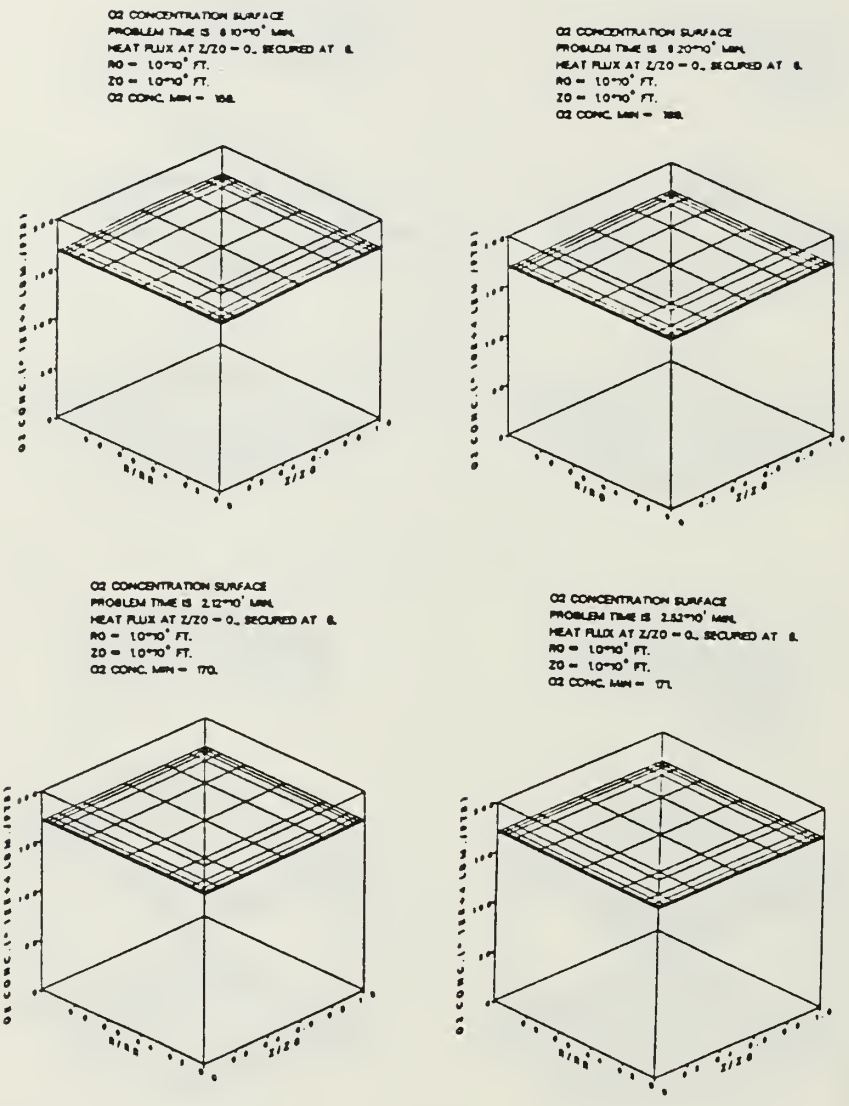

Figure 4.12 Model Rejecting Heat (Oxygen Concentration Profile)

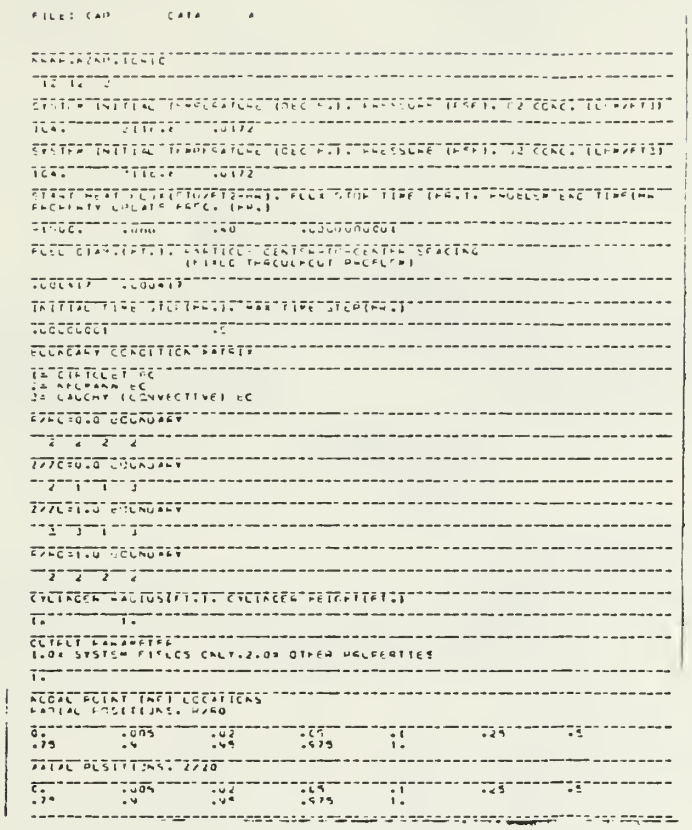

Figure 4.13 Accept/Reject Heat Problem Input Data Set

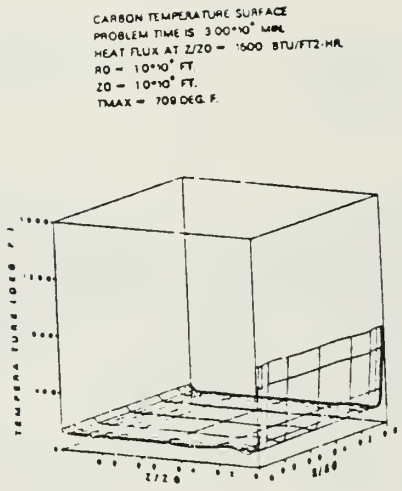

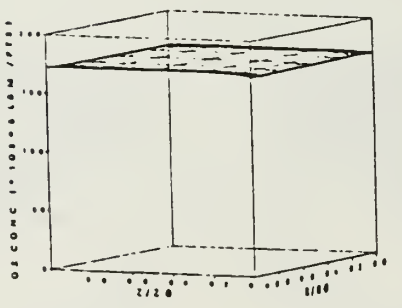

Figure 4.14 One Dimensional Problem (Carbon Temperature Profile and Oxygen Concentration Profile)

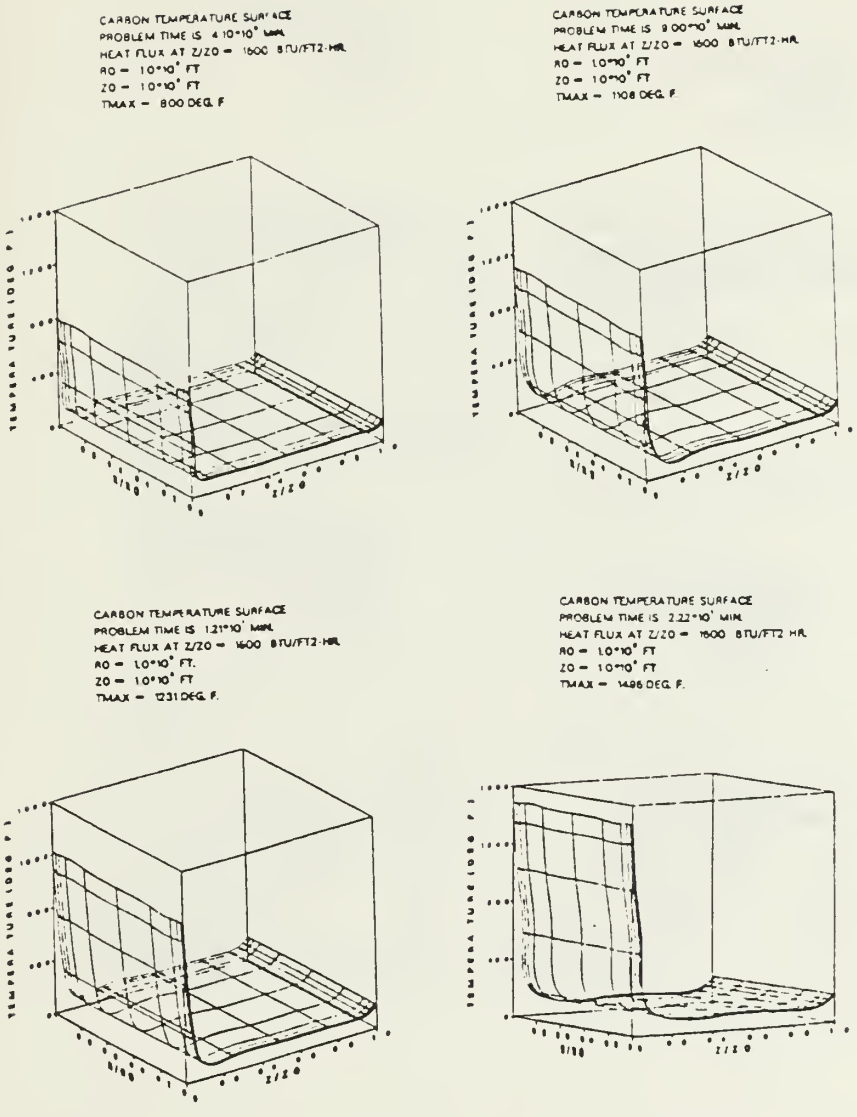

Figure 4.15 One Dimensional Problem (Carbon Temperature Profile)

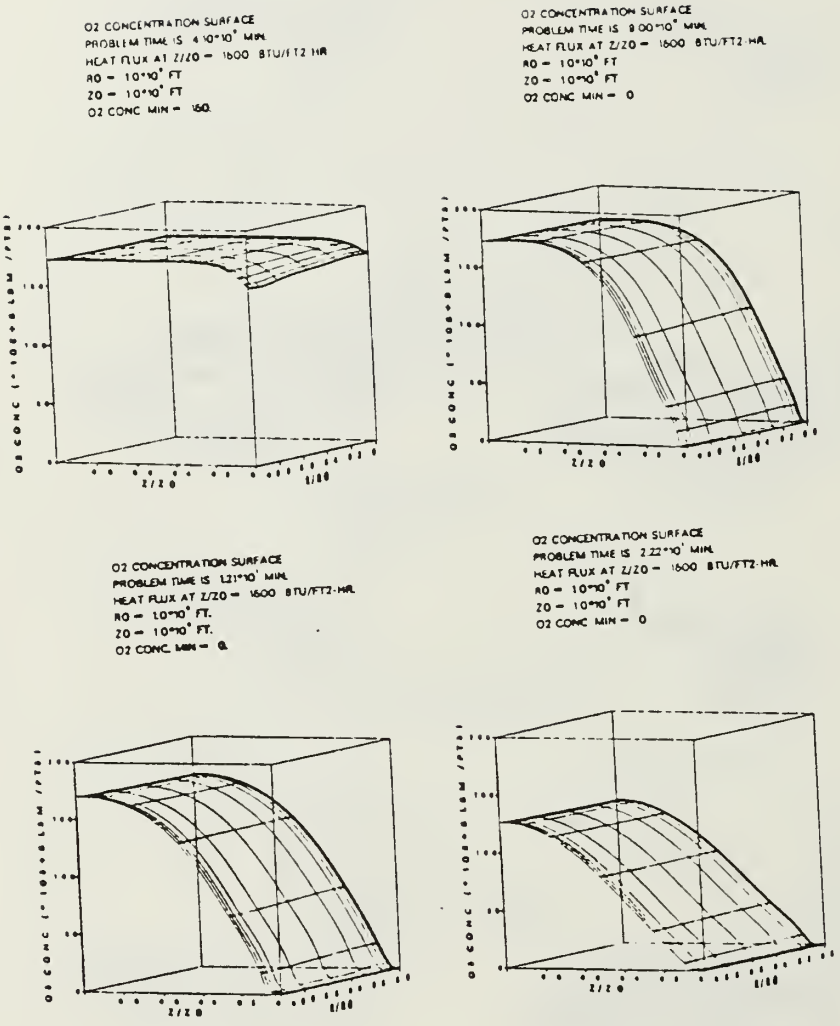

Figure 4.16 One Dimensional Problem (Oxygen Concentration Profile)

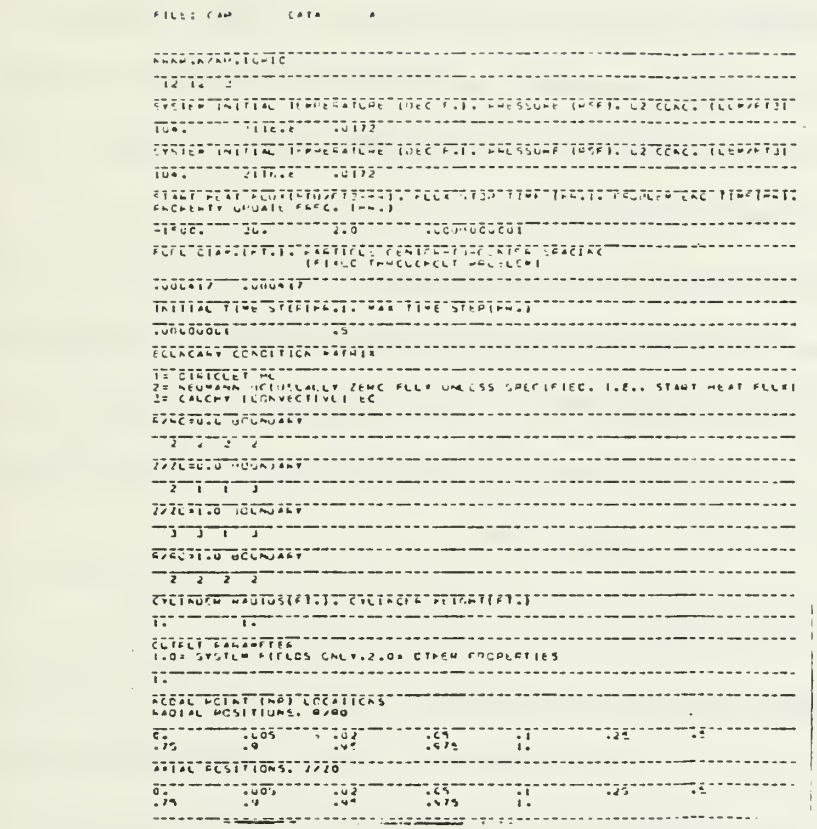

Figure 4.17 One Dimensional Problem Data Set

V. DISCUSSION AND CONCLUSIONS

Field problem behavior depends on three major factors: (1) Boundary conditions, (2) System excitation, and (3) The physical characteristics of the system.

Time limitations did not permit this investigator to conduct an exhaustive analysis of each of these factors. Some preliminary analyses were performed to obtain some understanding of the effect of boundary conditions, and excitation on system behavior.

There are a variety of physical parameters which govern system response, such as permeability, porosity, and the cylinder length-to-diameter ratio. Here only a brief investigation of the effect of porosity on system behavior was undertaken, and is reported.

A. BOUNDARY CONDITIONS

The boundary conditions used in the present investigation were presented in Chapter III. Other boundary conditions are possible. For example, if in place of Eqs. 3.32 and 3.36, an insulated boundary condition at $\frac{z}{z_o} = 1.0$ is imposed on the carbon and air temperatures, then preliminary results indicate temperature response is higher for equal values of time. This behavior is due to the buildup and storage of energy within the system associated with an insulated boundary.

Similarly, in place of Equation 3.44, a zero flux boundary condition at $\frac{z}{z_o} = 1.0$ could have been imposed on the oxygen concentration. The zero flux condition implies an impermeable boundary with respect to oxygen concentration fluxes. This boundary condition would apply to a very long cylinder (i.e., a regularity condition). In this investigation, a Cauchy (convective flux) boundary condition on the oxygen concentration is imposed at $\frac{z}{z_o} = 0.0$ and 1.0. As oxygen is locally consumed in the interior of the system, oxygen gradients are created. According to Fick's Law of Diffusion, a depleted oxygen region is replenished by the diffusion of oxygen from regions of relatively high concentration to regions of low concentration. Thus a convective flux boundary condition on oxygen causes the depletion of oxygen concentration to be retarded through the diffusion mechanism.

B. EXCITATIONS

The effects of high and low values of the heat flux applied at $\frac{z}{z_o} = 0.0$, are predictable. High values of heat flux lead to an accelerated development of both the carbon and air temperature profiles and O_2 concentration depletion within the system. For high values of heat flux at $\frac{z}{z_o} = 0.0$, the numerical integration scheme eventually slows noticeably as a result of steep gradients observed at this boundary.

C. PHYSICAL CHARACTERISTICS OF THE SYSTEM

The physical characteristics of the system generate a significant effect in field problem solutions. In the

problems discussed here the transport properties k_e, k_a, m/μ, $\mathcal{D}_e$ and the Arrhenius reaction rate term are governing factors in the respective field equations in which they appear. As previously discussed, the net balance between heat transfer rates and heat generation dictate whether a reaction will proceed to extinguishment or combustion. There are two time constants to be considered in a combustion problem of this type: a time constant for the Arrhenius reaction and a time constant associated with momentum transport. The momentum time constant affects the rate at which heat is convected (removed) out of a differential volume. The reaction time constant affects the rate at which heat is generated (added into) within a differential volume.

D. POROSITY ANALYSIS

In this problem there are many parameters one might vary in order to examine resultant system behavior. Due to time limitations this investigation examines the effect of one parameter, porosity, on system behavior. The observed effect of porosity values ranging from 0.476 to 0.90 is discussed. Of the nine runs attempted, only five had sufficient output data that allowed for comparative analyses. Employing Equation 3.1 for the porosity associated with spherical particles, the carbon diameter, d, was varied to achieve various values of porosity while holding the particle center-to-center distance D (Figure 3.1), fixed at

0.000417 ft. (0.005 in.). Values of d (ft.) equal to 0.000417, 0.000411, 0.000396, 0.000385 and 0.000370 were used to give values of porosity of 0.476, 0.5, 0.55, 0.60, and 0.65, respectively. The results are graphically presented in Figures 5.1--5.4. Figures 5.1 and 5.2 show the carbon temperature profile and the oxygen concentration profiles for porosity p_1 = 0.476 (D = 0.000417 ft. = 0.005 in.). In all cases, excitations for these runs are 1500 Btu/ft^2-hr (in) at $\frac{z}{z_o}$ = 0.0 and 50 Btu/ft^2-hr (out) at $\frac{r}{r_o}$ = 1.0; the pressure is 14.65 psi at $\frac{z}{z_o}$ = 0.0 and 14.55 at $\frac{z}{z_o}$ = 1.0; the cylinder length to diameter ratio is 0.5 (length = 1.0 ft.). Figures 5.1 and 5.2 represent typical graphical results for carbon temperature and oxygen concentration profiles. Figures 5.3 and 5.4 are a tabular summary of the results of the carbon temperature profile and the oxygen concentration profiles, respectively, for varying porosities. Profiles with higher values of initial porosity are observed to have accelerated development of temperature profiles (i.e., as the fuel diameters decrease (increasing porosity), the carbon temperature responds at a faster rate to system excitations). The oxygen concentration response is as expected (i.e., as reaction rate goes up, the oxygen concentration goes down). In the runs made for porosity values of 0.70, 0.75, 0.85 and 0.90, numerical difficulties were encountered. The temperature profiles were observed to increase sharply compared to lower values of porosity (300-400°

F in the first minute) at the $\frac{z}{z_o} = 0.0$ boundary. Due to the steep gradients, further system behavior could not be analyzed since output data consisted of a single output (T = 5-20 S., problem time, depending on porosity value) in 15 minutes of CPU time.

E. CONCLUSIONS

The combustion analysis program (CAP) is a viable tool for the analysis of heat transfer in porous media. The model constructed provides the user with the flexibility to solve problems with or without combustion. The role of the permeability model must not be underestimated. For it is the physical assumptions in this aspect of the model that govern the flow, heat transfer and in the end the evolution of the combustion problem.

F. RECOMMENDATIONS

Follow-on work is recommended in the following areas:

1. Develop a restart capability for the program which will allow for a problem to begin at any point in time with initial conditions and rate information being identical to previous timestep values.
2. Nondimensionalize equations in terms of other system quantities in addition to spatial dimensions.
3. Flex the model under other system parameters to examine effects on system behavior.

4. Consider an internal (particle-to-particle) radiative heat transfer analysis.

5. Consider other fuels and more detailed chemical kinetics chains.

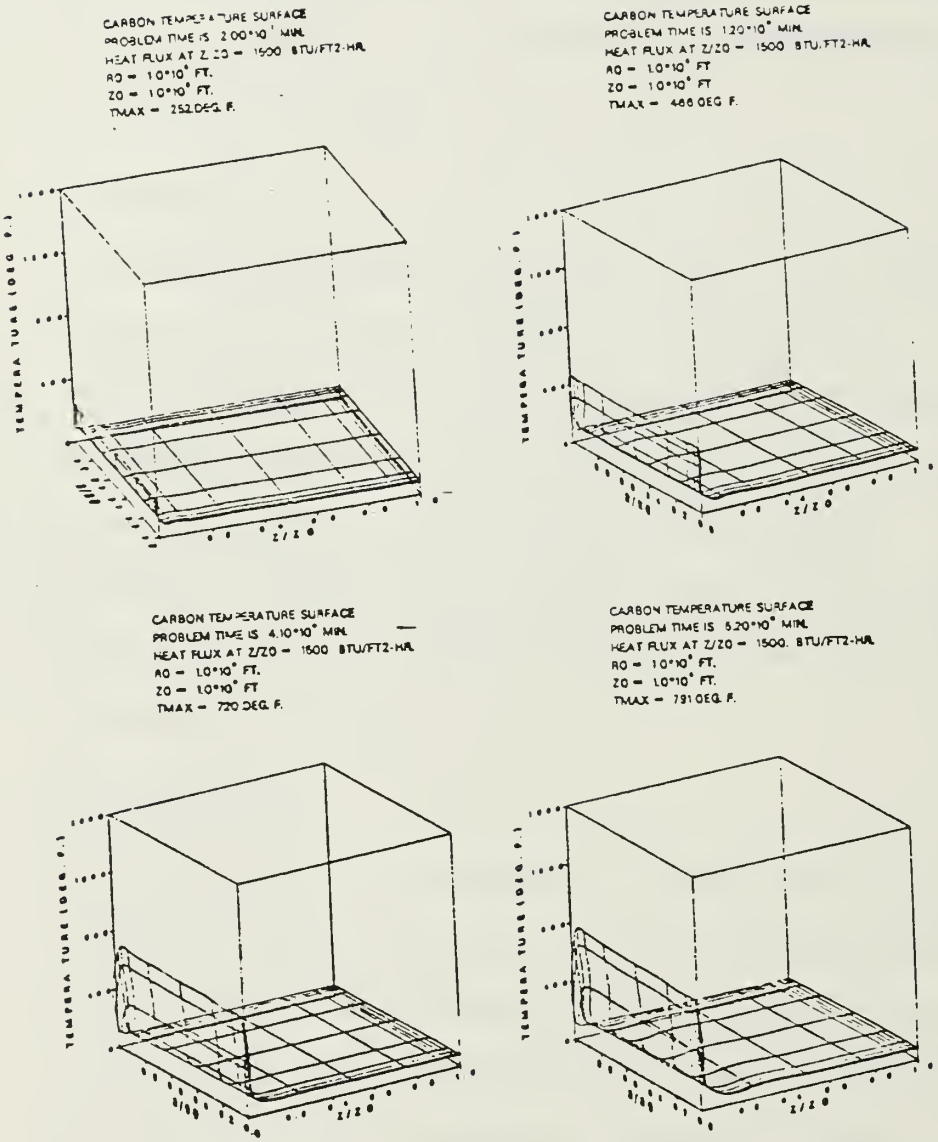

Figure 5.1 Carbon Temperature Profile (Porosity = 0.476) Radial Heat Flux (Out) 50-Btu/ft^2-hr

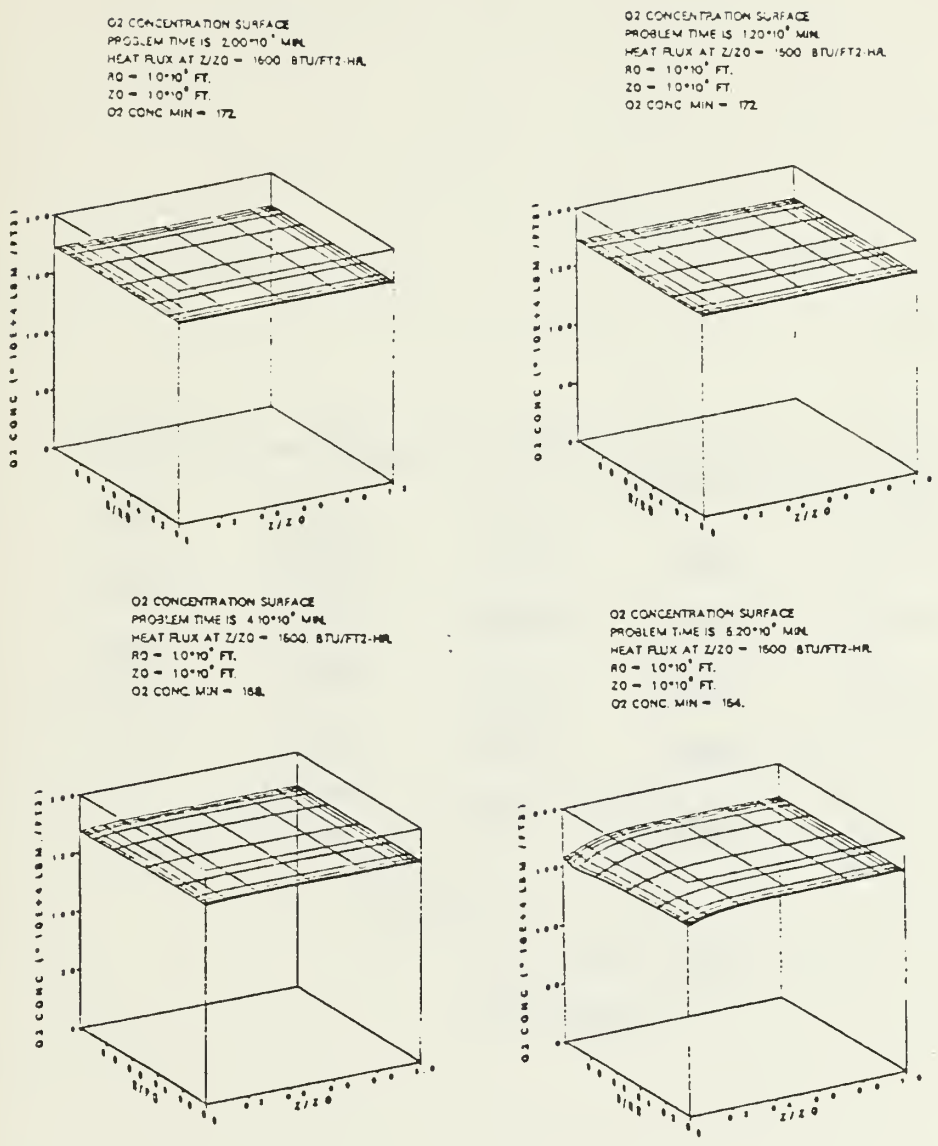

Figure 5.2 Oxygen Concentration (Porosity = 0.476)
Radial Heat Transfer (Out) 50 Btu/ft^2-hr

	t_1	t_2	t_3	t_4
P_1 :	207.0	466.0	*554.0	720.0
P_2 :	216.4	488.4	603.3	*765.0
P_3 :	239.2	563.0	695.0	905.0
P_4 :	266.0	632.0	*757.0	1034.0
P_5 :	294.6	724.8	*898.0	-

MAX Carbon Temp. (^{o}F)

* - interpolated

Figure 5.3 Maximum Carbon Temperature Summary Porosity: $p_1 = 0.476$, $p_2 = 0.5$, $p_3 = 0.55$, $p_4 = 0.60$, $p_5 = 0.65$. Time: $t_1 = 0.1$ minute, $t_2 = 1$ minute, $t_3 = 2$ minutes, $t_4 = 4$ minutes

	t_1	t_2	t_3	t_4
P_1	172.0	172.0	*171.5	168.0
P_2	172.0	172.0	172.0	*156.0
P_3	172.0	172.0	171.0	118.0
P_4	172.0	172.0	*157.0	26.6
P_5	172.0	171.0	*98.0	-

MIN O_2 % (($X\ 10^4$) lbm/ft^3)

* - interpolated

Figure 5.4 Oxygen Concentration Profile Summary Porosity: $p_1 = .476$, $p_2 = 0.5$, $p_3 = 0.55$, $p_4 = 0.60$, $p_5 = 0.65$. Time: $t_1 = 0.1$ minute, $t_2 = 1$ minute, $t_3 = 2$ minutes, $t_4 = 4$ minutes

APPENDIX A

FORMULATION OF FIELD EQUATIONS

A. PRESSURE DISTRIBUTION EQUATION

Darcy's law for two-dimensional flow is,

$$\underset{\sim}{Q} = -\frac{m}{\mu}\left(\frac{\partial p}{\partial r}\hat{r} + \left(\frac{\partial p}{\partial z} - p\,\rho_a\,g\right)\hat{z}\right) \tag{A.1}$$

where Q_r and Q_z are expressed as follows,

$$Q_r = -\frac{m}{\mu}\frac{\partial p}{\partial r} \tag{A.2}$$

$$Q_z = -\frac{m}{\mu}\left(\frac{\partial P}{\partial z} - p\,\rho_a\,g\right) \tag{A.3}$$

Invoking the Dupuit-Forcheimer relation, and solving for the pore velocity components u (radial velocity) and v (axial velocity), Equation A.1 becomes,

$$u = \frac{-m}{p\mu}\frac{\partial P}{\partial r} \tag{A.4}$$

$$v = \frac{-m}{p\mu}\left(\frac{\partial P}{\partial z} - p\,\rho_a\,g\right) \tag{A.5}$$

The continuity relation (derived in Appendix B) is,

$$\frac{D(p\rho_a)}{Dt} + p\,\rho_a\,\mathrm{Div}\,\vec{V} = 0 \tag{A.6}$$

Substituting Equation A.2 and Equation A.3 into Equation A.6 yields,

$$\frac{\partial p\,\rho_a}{\partial t} = p\,\rho_a \vec{\nabla}\cdot\left(\frac{m}{p\mu}\left(\frac{\partial P}{\partial r}\hat{r} + \left(\frac{\partial P}{\partial z} - p\,\rho_a g\right)\hat{z}\right)\right) + \frac{m}{p\mu}\left(\frac{\partial P}{\partial r}\hat{r} + \left(\frac{\partial P}{\partial z} - p\,\rho_a g\right)\hat{z}\right)\cdot\nabla p\,\rho_a \qquad (A.7)$$

Expanding terms, Equation A.7 becomes,

$$\frac{\partial^2 P}{\partial r^2} + \frac{\partial^2 P}{\partial z^2} + \left(\frac{1}{\rho_a}\frac{\partial \rho_a}{\partial r} + \frac{1}{m}\frac{\partial m}{\partial r} - \frac{1}{\mu}\frac{\partial \mu}{\partial r} + \frac{1}{r}\right)\frac{\partial P}{\partial r} + \left(\frac{1}{\rho_a}\frac{\partial \rho_a}{\partial z} + \frac{1}{m}\frac{\partial m}{\partial z} - \frac{1}{\mu}\frac{\partial \mu}{\partial z}\right)\left(\frac{\partial P}{\partial z} + p\,\rho_a g\right) = \frac{\mu}{\rho_a m}\frac{\partial P \rho_a}{\partial t} \qquad (A.8)$$

Equation A.7 with associated boundary conditions (presented in Section II.B) is cast into a finite element formulation and becomes one of four field equations. Pressure gradient information is then substituted into Equation A.4 and Equation A.5 to obtain the pore velocity components.

B. POROUS SOLID HEAT TRANSFER EQUATION

In performing energy balances on both the porous solid and on the air, a differential volume of porous medium may be partitioned into respective volumes, $dV_s = (1-p)dV$ for the solid, and $dV_a = pdV$ for the air (shown in Figure A.1). The convention used for the energy balance of an arbitrary differential volume, dV, is,

Heat into DV + Heat generation = Heat out of DV

+ Increase in internal energy (A.9)

The heat transfer mechanisms considered for the carbon are conduction, radiation heat transfer between particles, convection heat transfer from the particles to the air, and heat generation. Applying the above convention, the energy balance on a differential volume of porous solid is (invoking Tayler Series expansions and neglecting higher order terms),

$$\left[-\frac{1}{r}\frac{\partial}{\partial r}((1-p)rq_{cond,r}) - \frac{\partial}{\partial z}((1-p)q_{cond,z})\right.$$

$$\left. - \frac{1}{r}\left(\frac{\partial}{\partial r}((1-p)rq_{rad,r}) - \frac{\partial}{\partial z}((1-p)q_{rad,z})\right)\right]dV$$

$$- q_{conv}dA' + q_{gen}dA' = (1-p)\dot{q}_{int}dV \qquad (A.10)$$

In vector form, Equation A.10 becomes,

$$-\vec{\nabla}\cdot(q_{cond} + q_{rad})dV - q_{conv}dA' + q_{gen}dA' = (1-p)\dot{q}_{int}dV \qquad (A.11)$$

Substituting the following expressions into Equation A.10,

$$q_{cond} = -k_e\nabla T_c \qquad \text{Fourier's law} \qquad (A.12)$$

$$q_{rad} = -k_r \nabla T_c \quad^{*} \qquad \text{Fourier analogy (radiative)} \qquad \text{(A.13)}$$

$$q_{conv} = h(T_c - T_a) \qquad \text{Newton's Cooling Law} \qquad \text{(A.14)}$$

$$q_{gen} = R_g \qquad \text{Heat generation} \qquad \text{(A.15)}$$

$$q_{int} = \rho_c C_c \frac{\partial T}{\partial t} \qquad \text{Internal energy} \qquad \text{(A.16)}$$

yields,

$$\frac{1}{r}\{\frac{\partial}{\partial r}(r(1-p)(k_e)\frac{\partial T_c}{\partial r}) + \frac{\partial}{\partial z}((1-p)(k_e)\frac{\partial T_c}{\partial z})\}dV$$

$$- h(T_c - T_a)dA' + R_g dA' = (1-p)\rho_c C_c \frac{\partial T}{\partial t} dV \qquad \text{(A.17)}$$

Dividing through by dV, and defining dA'/dV as Z, the specific internal area (i.e., surface area per unit volume), Equation A.17 becomes,

$$\vec{\nabla}\cdot((1-p)(k_e)\nabla T_c) - hZ(T_c - T_a) + R_g Z = (1-p)\rho_c C_c \frac{\partial T}{\partial t} \qquad \text{(A.18)}$$

The expressions used to obtain values of the properties and parameters in Equation A.18 are presented in Section III.E.

C. AIR HEAT TRANSFER EQUATION

The formulation of the air heat transfer equation begins with the general two-dimensional energy balance equation,

---

*The difficulty in obtaining an expression for k_r is addressed in Section III.E. Throughout this work, one may keep in mind that k_e should really be $(k_e + k_r)$ to account for conduction as well as radiation within the porous medium.

$$\frac{p\,\rho_a\,D(U+K)}{Dt} = -\vec{\nabla}\cdot pq - \vec{\nabla}\cdot pP\vec{V} - (\vec{\nabla}\cdot(p\vec{\tau}\cdot\vec{V})) + hZ(T_c - T_a) + p\,\rho_a(\vec{V}\cdot g) \qquad (A.19)$$

where U is the internal energy, K is kinetic energy, τ is the dissipation function, and g is the gravitational acceleration. Expansion of Equation A.19 yields,

$$p\,\rho_a\frac{D}{Dt}(e+\tfrac{1}{2}(u^2+v^2)) = -\vec{\nabla}\cdot(-pk_a\nabla T_a) - \vec{\nabla}\cdot(p\,P\vec{V}) - \sum_i\sum_j \frac{\partial}{\partial x_i}\,p\,\tau_{ij}V_j + hZ(T_c - T_a) + p\,\rho_a\,v\,g \qquad (A.20)$$

where

$$\vec{\nabla}(p\vec{\tau}\cdot\vec{V}) = \sum_i\sum_j \frac{\partial}{\partial x_i}\,p\,\tau_{ij}V_j = \vec{\nabla}(p\tau_{rr}V_r + p\tau_{rz}V_z + p\tau_{zr}V_r + p\tau_{zz}V_z)$$

$$= \frac{\partial}{\partial r}(p\tau_{rr}u + p\tau_{rz}v) + \frac{\partial}{\partial z}(p\tau_{zr}u + p\tau_{zz}v) \qquad (A.21)$$

And so Equation A.19 becomes,

$$p\rho_a[\frac{De}{Dt} + \frac{D}{dt}(\frac{1}{2}(u^2+v^2)] = \vec{\nabla}\cdot(pk_a\nabla T_a) - \frac{\partial}{\partial r}(p\tau_{rr}u + p\,\tau_{rz}v) - \frac{\partial}{\partial z}(p\tau_{zr}u + p\tau_{zz}v) - (\nabla pP\cdot\vec{V} + pP\vec{\nabla}\cdot\vec{V}) + hZ(T_c - T_a) + p\,\rho_a\,v\,g\ . \qquad (A.22)$$

As in the porous solid heat transfer equation, the time and position dependent porosity appears inside the differential. Expanding terms, the air energy equation becomes,

$$p\,\rho_a \frac{De}{Dt} + \frac{p\rho_a}{2}\frac{D}{Dt}(u^2+v^2) = \vec{\nabla}\cdot(p\,k_a \nabla T_a) - [\nabla p P\cdot\vec{V} + p\,P\,\vec{\nabla}\cdot\vec{V}]$$

$$- \frac{\partial}{\partial r}(p\tau_{rr}u + p\tau_{rz}v)$$

$$- \frac{\partial}{\partial z}(p\tau_{rz}u + p\tau_{zz}v) + h^Z(T_c - T_a)$$

$$+ p\,\rho_a v\,g\,. \qquad \text{(A.23)}$$

Consider the momentum equation for the r-direction,

R Momentum

$$\frac{\partial}{\partial t}(p\,\rho_a u) = \frac{1}{r}(-\frac{\partial}{\partial r}(r\,p\rho_a u^2) - \frac{\partial}{\partial z}(p\,\rho_a uv) - \frac{\partial pP}{\partial r}$$

$$- (\frac{1}{r}\frac{\partial}{\partial r}(p\,r\,\tau_{rr}) - \frac{p\tau_{\theta\theta}}{r} + \frac{\partial}{\partial z}(p\,\tau_{rz})) \qquad \text{(A.24)}$$

Consider the momentum equation for the z-direction,

Z Momentum

$$\frac{\partial}{\partial t}(p\,\rho_a v) = \frac{1}{r}(-\frac{\partial}{\partial r}(r\,p\rho_a uv) - \frac{\partial}{\partial z}(p\,\rho_a v^2) - \frac{\partial}{\partial z}(pP)$$

$$- (\frac{1}{r}\frac{\partial}{\partial r}(p\,\tau_{rz}) + \frac{\partial}{\partial z}(p\,\tau_{zz})) + p\,\rho_a g \qquad \text{(A.25)}$$

and the continuity equation,

Continuity

$$\frac{\partial}{\partial t}(p\rho_a) = - u\frac{\partial}{\partial r}(p\rho_a) - (p\,\rho_a\frac{\partial u}{\partial r} + \frac{p\,\rho_a u}{r}) - v\,\frac{\partial p\rho_a}{\partial z}$$

$$- p\,\rho_a\,\frac{\partial v}{\partial z} \qquad \text{(A.26)}$$

Multiplying the continuity equation through by u, and substituting this into Equation A.24, the r-momentum equation becomes,

$$p\,\rho_a\frac{\partial u}{\partial t} = - p\rho_a\,u\frac{\partial u}{\partial r} - p\,\rho_a v\,\frac{\partial u}{\partial z} - \frac{\partial pP}{\partial r}$$

$$- (\frac{1}{r}\,\frac{\partial}{\partial r}(p\,r\,\tau_{rr}) - \frac{p\tau_{\theta\theta}}{r} + \frac{\partial}{\partial z}(p\,\tau_{rz})) \qquad \text{(A.27)}$$

Multiplying Equation A.26 by v, and substituting this into Equation A.25, the z-momentum equation becomes,

$$p\rho_a\,\frac{\partial v}{\partial t} = - p\,\rho_a\,u\frac{\partial v}{\partial r} - p\,\rho_a v\,\frac{\partial v}{\partial z} - \frac{\partial pP}{\partial z} - (\frac{1}{r}\,\frac{\partial}{\partial r}(p\,r\,\tau_{rz})$$

$$+ \frac{\partial}{\partial z}(p\,\tau_{zz})) + p\,\rho_a\,g \qquad \text{(A.28)}$$

Multiplying Equation A.27 by u and noting that,

$$p\,\rho_a\,u\,\frac{Du}{Dt} = p\,\rho_a\,u\,\frac{\partial u}{\partial t} + p\,\rho_a\,u^2\,\frac{\partial u}{\partial r} + p\,\rho_a\,uv\,\frac{\partial u}{\partial z} \qquad \text{(A.29)}$$

Equation A.27 becomes,

$$p\,\rho_a\,u\,\frac{Du}{Dt} = -u\,\frac{\partial pP}{\partial r} - u\left(\frac{1}{r}\,\frac{\partial}{\partial r}(p\,r\tau_{rr}) - \frac{p\tau_{\theta\theta}}{r} + \frac{\partial}{\partial z}(p\,\tau_{rz})\right) \tag{A.30}$$

Multiplying Equation A.28 by v and noting that,

$$p\,\rho_a\,v\,\frac{Dv}{Dt} = p\,\rho_a\,v\,\frac{\partial v}{\partial t} + p\,\rho_a\,u\,v\,\frac{\partial v}{\partial r} + p\,\rho_a\,v^2\,\frac{\partial v}{\partial z} \tag{A.31}$$

Equation A.28 becomes

$$p\,\rho_a\,v\,\frac{Dv}{Dt} = -v\,\frac{\partial pP}{\partial z} - v\left(\frac{1}{r}\,\frac{\partial}{\partial r}(p\,r\tau_{rz})\right) + \frac{\partial}{\partial z}(p\tau_{zz})) + p\,\rho_a\,v\,g \tag{A.32}$$

Expanding Equation A.30 yields,

$$p\,\rho_a\,u\,\frac{Du}{Dt} = -u\,\frac{\partial pP}{\partial r} - u\,\frac{\partial p\tau_{rr}}{\partial r} - \frac{u}{r}\,p\tau_{rr} + \frac{up\tau_{\theta\theta}}{r} - u\,\frac{\partial}{\partial z}(p\tau_{rz}) \tag{A.33}$$

Expanding Equation A.32 yields,

$$p\,\rho_a\,v\,\frac{Dv}{Dt} = -v\,\frac{\partial pP}{\partial z} - v\,\frac{\partial(p\tau_{rz})}{\partial r} - \frac{v}{r}\,p\,\tau_{rz} - V\,\frac{\partial}{\partial z}(p\tau_{zz}) + p\,\rho_a\,v\,g \tag{A.34}$$

The energy Equation A.23, after substituting and expanding terms, is,

$$p\rho_a \frac{De}{Dt} + p\rho_a u \frac{Du}{Dt} + p\rho_a v \frac{Dv}{Dt} = \vec{\nabla}\cdot(pk_a \nabla T_a) - (p\tau_{rr}\frac{\partial u}{\partial r}$$

$$+ u \frac{\partial(p\tau_{rr})}{\partial r} + p\tau_{rz}\frac{\partial v}{\partial r}$$

$$+ v \frac{\partial}{\partial r}(p\tau_{rz})) - (p\tau_{zr}\frac{\partial u}{\partial z}$$

$$+ u \frac{\partial}{\partial z}(p\tau_{zr}) + p\tau_{zz}\frac{\partial v}{\partial z}$$

$$+ v \frac{\partial}{\partial z}(p\tau_{zz})) - (\vec{\nabla}pP\cdot\vec{V}$$

$$+ p P \vec{\nabla}\cdot\vec{V}) + p\rho_a v g$$

$$+ hZ(T_c - T_a) \qquad \text{(A.35)}$$

Substituting Equation A.33 and Equation A.34 into Equation A.35 yields,

$$p\rho_a \frac{De}{Dt} = \vec{\nabla}\cdot(pk_a\nabla T_a) - p P \text{Div}\ \vec{V} + hZ(T_c - T_a)$$

$$- (p\tau_{rr}\frac{\partial u}{\partial r} + p\tau_{rz}\frac{\partial v}{\partial r} + p\tau_{zr}\frac{\partial u}{\partial z} + p\tau_{zz}\frac{\partial v}{\partial z})$$

$$- \frac{u p\tau_{\theta\theta}}{r} + \frac{u}{r}p\tau_{rr} + \frac{v}{r}p\tau_{rz} \qquad \text{(A.36)}$$

The viscous dissipation terms in Expression A.36 are neglected because the fluid is a gas flowing at low velocity (see [Ref. 9]). Therefore, the energy equation for the air in the porous medium is,

$$p\,\rho_a \frac{De}{Dt} = \nabla\cdot(pk_a \nabla T_a) - p\,P\,Div\,\vec{V} + hZ(T_c - T_a) \qquad (A.37)$$

With specific enthalpy for a gas defined by,

$$h = e + \frac{P}{\rho} \qquad (A.38)$$

De/Dt can be expressed as,

$$\frac{De}{Dt} = \frac{Dh}{Dt} - \frac{1}{\rho_a}\frac{DP}{Dt} + \frac{P}{\rho_a^2}\frac{D\rho_a}{Dt} \qquad (A.39)$$

where h is the specific enthalpy, and e is the specific energy (internal plus kinetic). Multiplying the continuity equation through by $P/(p\rho_a^2)$ obtains,

$$\frac{P}{p\rho_a^2}\frac{\partial}{\partial t}(p\rho_a) + \frac{P}{p\rho_a^2}\frac{1}{r}\frac{\partial}{\partial r}(p\,\rho_a\,r\,u) + \frac{P}{p\rho_a^2}\frac{\partial}{\partial z}(p\,\rho_a\,v) = 0\,. \qquad (A.40)$$

Expanding yields,

$$\frac{P}{p\rho_a^2}\left(p\frac{\partial\rho_a}{\partial t} + \rho_a\frac{\partial p}{\partial t}\right) = -\frac{P}{p\rho_a^2}u\frac{\partial}{\partial r}(p\rho_a) - \frac{P}{p\rho_a^2}\frac{p\rho_a}{r}\frac{\partial}{\partial r}(ru)$$

$$- \frac{P\,v}{p\rho_a^2}\frac{\partial}{\partial z}(p\rho_a) - \frac{P}{p\rho_a^2}p\,\rho_a\frac{\partial v}{\partial z} \qquad (A.41)$$

In vector notation, Equation A.41 becomes,

$$\frac{P}{\rho_a^2}\frac{\partial \rho_a}{\partial t} + \frac{P}{p\rho_a}\frac{\partial p}{\partial t} = -\frac{P}{\rho_a^2}(\vec{V}\cdot\nabla)\rho_a - \frac{P}{p\rho_a}(\vec{V}\cdot\vec{\nabla})p$$

$$- \frac{P}{\rho_a}\,\mathrm{Div}\,\vec{V} \qquad \text{(A.42)}$$

Employing Stokes (substantial) derivative notation, Equation A.42 becomes,

$$\frac{P}{\rho_a^2}\frac{D\rho_a}{Dt} = -\frac{P}{p\rho_a}\frac{Dp}{Dt} - \frac{P}{\rho_a}\,\mathrm{Div}\,\vec{V} \qquad \text{(A.43)}$$

Substituting Equation A.43 into Equation A.39 yields,

$$\frac{De}{Dt} = \frac{Dh}{Dt} - \frac{1}{\rho_a}\frac{DP}{Dt} - \frac{P}{\rho_a}\,\mathrm{Div}\,\vec{V} - \frac{P}{p\rho_a}\frac{Dp}{Dt} \qquad \text{(A.44)}$$

Substituting Equation A.44 into Equation A.37 yields,

$$p\rho_a\frac{Dh}{Dt} - p\frac{DP}{Dt} - P\frac{Dp}{Dt} = \vec{\nabla}\cdot(p\,k_a\nabla T_a) + hZ(T_c - T_a) \qquad \text{(A.45)}$$

Simplification yields,

$$p\,\rho_a\frac{Dh}{Dt} - \frac{DpP}{Dt} = \vec{\nabla}\cdot(p\,k_a\nabla T_a) + hZ(T_c - T_a) \qquad \text{(A.46)}$$

Invoking the Maxwell relations for a simple compressible substance,

$$dh = T\,ds + \frac{1}{\rho}\,dP \qquad \text{(A.47)}$$

$$ds = C_p \frac{dT}{T} - \frac{\beta}{\rho} dP \tag{A.48}$$

and recalling that,

$$\beta = -\frac{1}{\rho} \frac{\partial \rho}{\partial T})_p \tag{A.49}$$

the equation of state for a perfect gas,

$$P = \rho RT \tag{A.50}$$

simplifies Equation A.49 such that,

$$\beta = -\frac{RT}{P}\left(\frac{-P}{RT^2}\right) = \frac{1}{T} \tag{A.51}$$

Thus, Equation A.48 becomes,

$$ds = C_p \frac{dT}{T} - \frac{1}{\rho T} dP \tag{A.52}$$

Substituting Equation A.52 into Equation A.47 and cancelling terms yields,

$$-dh = C_p \, dT \tag{A.53}$$

or

$$\frac{Dh}{Dt} = C_a \frac{DT_a}{Dt} \tag{A.54}$$

Substituting Equation A.54 into Equation A.45 yields,

$$p\,\rho_a C_a \frac{\partial T_a}{\partial t} = \vec{\nabla}\cdot(pk_a \nabla T_a) - p\,\rho_a C_a(\vec{V}\cdot\vec{\nabla})T_a + hZ(T_c - T_a) + \frac{D(pP)}{Dt} \quad (A.55)$$

Making the assumption that pP changes very little with time [Ref. 9], (this assumption was subsequently confirmed by the model), i.e.,

$$\frac{DpP}{Dt} \approx (V\cdot\nabla)pP = u\frac{\partial(pP)}{\partial r} + v\frac{\partial(pP)}{\partial z} \quad (A.56)$$

The final air heat transfer (energy conservation) equation is,

$$p\,\rho_a C_a \frac{\partial T_a}{\partial t} = \vec{\nabla}\cdot(pk_a \nabla T_a) - p\,\rho_a C_a(\vec{V}\cdot\nabla)T_a + u\frac{\partial pP}{\partial r} + v\frac{\partial pP}{\partial z} + hZ(T_c - T_a) \quad (A.57)$$

In vector form, Equation A.57 becomes,

$$p\,\rho_a C_a \frac{\partial T_a}{\partial t} = \vec{\nabla}\cdot(pk_a \nabla T_a) - p\,\rho_a C_a(\vec{V}\cdot\nabla)T_a + (\vec{V}\cdot\nabla)pP + hZ(T_c - T_a) \quad (A.58)$$

The expressions used to obtain the properties and parameters in the coefficients of Equation A.57 are presented in Section III.E.

D. OXYGEN MOLECULE DIFFUSION EQUATION

The final consideration in formulating the field equations for the model is the transport of oxygen molecules. The oxygen molecule transport equation is obtained by a conservation of species balance on the differential volume of air, dV = pdV. The convention used for the species balance into a differential volume is,

$$O_2 \text{ in} = O_2 \text{ out} + O_2 \text{ consumed} + O_2 \text{ accumulated} \tag{A.59}$$

The transport mechanisms considered were diffusion due to concentration gradients (Fick's law), convection, and air consumption by combustion. The species balance on oxygen becomes,

$$\begin{aligned} &\dot{pm}_{diff}dA\Big|_r + \dot{pm}_{diff}dA\Big|_z + \dot{pm}_{conv}dA\Big|_r + \dot{pm}_{conv}dA\Big|_z \\ &= \dot{pm}_{diff}dA\Big|_{r+dr} + \dot{pm}_{diff}dA\Big|_{z+dz} + \dot{pm}_{conv}dA\Big|_{r+dr} \\ &\quad + \dot{pm}_{conv}dA\Big|_{z+dz} + \dot{m}_{cons}dA' + \dot{pm}_{acc}dV \end{aligned} \tag{A.60}$$

Representing terms on the right side by Taylor series expansions (neglecting higher order terms), i.e.,

$$\dot{pm}_k dA\Big|_{\varepsilon_i+d\varepsilon_i} = \dot{pm}_k dA\Big|_{\varepsilon_i} + \frac{\partial}{\partial \varepsilon_i}(\dot{pm}_k dA)d\varepsilon_i \tag{A.61}$$

where,

$$k = conv, \quad \varepsilon_i = r \text{ or } z \qquad dA_r = r\, d\theta\, dZ \tag{A.62}$$

$$\text{and} \quad dA_z = r\, dr\, d\theta \tag{A.63}$$

Then Equation A.61 becomes,

$$\frac{\partial}{\partial r}(p\, \dot{m}\, dA_r)\, dr = \frac{\partial}{\partial r}(r\, p\, u\, \phi\, d\theta\, dz)\, dr$$

$$= \frac{1}{r}\, \frac{\partial}{\partial r}(r\, p\, u\, \phi)\, r\, d\theta\, dZ\, dr \tag{A.64}$$

and

$$\frac{\partial}{\partial z}(p\, \dot{m}\, dA_z)\, dz = \frac{\partial}{\partial z}(p\, v\, \phi\, r\, dr\, d\theta)\, dz$$

$$= \frac{\partial}{\partial z}(p\, v\, \phi)\, r\, d\theta\, dz\, dr \tag{A.65}$$

Substituting Equations A.64 and A.65 into Equation A.60, cancelling terms and rearranging, Equation A.61 becomes,

$$-\frac{\partial}{\partial r}(p(\dot{m}_{diff} + \dot{m}_{conv})\, dA_r)\, dr - \frac{\partial}{\partial z}(p(\dot{m}_{diff} + \dot{m}_{conv})\, dA_z)\, dz$$

$$- \dot{m}_{cons} dA' = p\dot{m}_{acc} dV \tag{A.66}$$

Substituting the following expressions into Equation A.66,

$$\dot{m}_{diff} = - \mathcal{D}_e \nabla \phi \tag{A.67}$$

$$\dot{m}_{conv,r} = u\phi, \qquad \dot{m}_{conv,z} = v\phi \tag{A.68}$$

$$\dot{m}_{cons} = R_{O_2} \tag{A.69}$$

$$\dot{m}_{acc} = \frac{\partial \phi}{\partial t} \tag{A.70}$$

dividing both sides by dV, and letting dA'/dV equal the specific internal area, z, the oxygen molecule diffusion equation becomes,

$$\vec{\nabla} \cdot (p \mathcal{D}_e \nabla \phi) - \vec{\nabla} \cdot (p \phi \vec{V}) - R_{O_2} z = \frac{p \partial \phi}{\partial t} \tag{A.71}$$

The methods and expressions for obtaining the properties and parameters in the coefficients of Equation A.71 are presented in Section III.G.

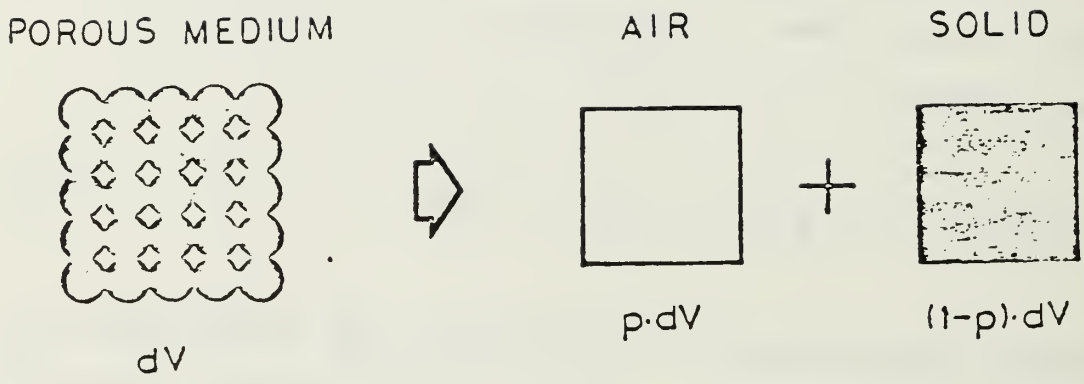

Figure A.1 Separating A Differential Volume of Porous Medium into Respective Volumes of Solid and Air

APPENDIX B

AUXILIARY EQUATION FORMULATION

A. CONTINUITY EQUATION

The continuity equation for a fluid in a porous medium is expressed by,

$$\frac{D(p\rho_a)}{Dt} + p\,\rho_a \,\mathrm{Div}\,\vec{V} = 0 \qquad (B.1)$$

or in equivalent form,

$$\frac{\partial}{\partial t}(p\rho_a) + (\vec{V}\cdot\nabla)p\rho_a + p\rho_a(\vec{\nabla}\cdot\vec{V}) = 0 \qquad (B.2)$$

and

$$\frac{\partial}{\partial t}(p\rho_a) + u\,\frac{\partial p\rho_a}{\partial r} + v\,\frac{\partial(p\rho_a)}{\partial z} + p\rho_a\left(\frac{1}{r}\,\frac{\partial(ru)}{\partial r} + \frac{\partial v}{\partial z}\right) \qquad (B.3)$$

B. LAGRANGE POLYNOMIAL APPROXIMATIONS FOR THERMAL PROPERTIES

Relations for calculating the dynamic viscosity, thermal conductivity, and specific heat at constant pressure of air at different temperatures were required. Second order Lagrange polynomial fits to empirical data provide a simple method for obtaining the relations required. Vatikiotis [Ref. 9] gives the details for arriving at the resulting set of polynomials,

$$\mu = -3.308 \times 10^{-9} T_A^2 + 4.633 \times 10^{-5} T_a + 4.427 \times 10^{-2} \quad \text{(B.12)}$$

$$k_a = -2.608 \times 10^{-10} T_a^2 + 1.930 \times 10^{-5} T_a + 1.361 \times 10^{-2} \quad \text{(B.13)}$$

$$C_a = -1.293 \times 10^{-9} T_a^2 + 2.758 \times 10^{-5} T_a + .238 \quad \text{(B.14)}$$

Each expression obtains property values within two percent of the data presented in [Ref. 9] for temperatures up to 3000 degrees Fahrenheit.

C. CARBON PARTICLE SURFACE RECESSION

The following analysis of particle diameter consumption assumes that the fuel particle surface recedes uniformly. This assumption is reasonable if the particle diameter is small in comparison to the cylinder geometry, i.e., negligible boundary effects. In addition, since the velocities are low, the hydrodynamic effects on the uniformity of the particle surface recession are negligible. The analysis also assumes there are no significant thermal gradients within the particle, i.e., an isothermal carbon particle. This is also reasonable for the small particles examined in this analysis. A mass balance must be performed on the particle and equated with the reaction rate. This equivalence yields the following expression,

$$\frac{dm}{dt} = R_c Z \quad \text{(B.15)}$$

or equivalently,

$$\frac{d(1-p)\rho_c}{dt} = R_c Z \qquad \text{(B.15a)}$$

Simplification of Equation B.15a yields,

$$-\frac{dp}{dt} = \frac{R_c Z}{\rho_c} \qquad \text{(B.16)}$$

Substituting the porosity expression for spherical particles yields,

$$\frac{d}{dt}\left(\frac{\pi}{6}\left(\frac{d}{D}\right)^3\right) = \frac{R_c Z}{\rho_c} \qquad \text{(B.17)}$$

Application of the time operator yields,

$$-\frac{3}{6}\pi d^2 \frac{\dot{d}}{D^3} = \frac{R_c Z}{\rho_c} \qquad \text{(B.18)}$$

Isolating the diameter time derivative yields,

$$\dot{d} = \frac{-2 R_c Z D^3}{\rho_c \pi d^2} \qquad \text{(B.19)}$$

APPENDIX C

GALERKIN FEM FORMULATION

A. FINITE ELEMENT METHOD

The solution of the system of coupled, nonlinear partial differential equations given by Equations 3.9, 3.22, 3.26 and 3.27 — subject to boundary and initial conditions, was obtained by a Galerkin formulation of the Finite Element Method.

1. Galerkin Formulation

A Galerkin formulation of the Finite Element Method was used to obtain solutions of the porous solid and air energy equations, the oxygen diffusion equation, and the continuity (pressure--Darcy's law) equation. A convenient form of Equations 3.9, 3.22, 3.26 and 3.27 was used in the formulation where the spacial coordinates, r and z were nondimensionalized by $\varepsilon = z/z_o$ and $\eta = r/r_o$.

The closed domain defined in (r,z) space by (0,0), (0,1), (1,1), and (1,0) was partitioned into NEL (2*(NRNP-1)*(NZNP-1)) contiguous area elements obtained from a NSNP model. NSNP, NRNP and NZNP are the number of system nodal points, radial points, and axial points, respectively. The four field variables T_c, T_a, P and were approximated by,

$$T_c = \psi_{1j}(\eta,\varepsilon,t) = \sum_{i=1}^{NSNP} N_j(\eta,\varepsilon)\theta_{1j}(t) \qquad (C.1)$$

$$T_a = \psi_{2j}(\eta,\varepsilon,t) = \sum_{j=1}^{NSNP} N_j(\eta,\varepsilon)\theta_{2j}(t) \qquad (C.2)$$

$$P = \psi_{3j}(\eta,\varepsilon,t) = \sum_{j=1}^{NSNP} N_j(\eta,\varepsilon)\theta_{3j}(t) \qquad (C.3)$$

$$\phi = \psi_{4j}(\eta,\varepsilon,t) = \sum_{j=1}^{NSNP} N_j(\eta,\varepsilon)\theta_{4j}(t) \qquad (C.4)$$

where N_j for j = 1,...,NSNP is a set of specified linear basis functions with local support, and the sets θ_{1j}, θ_{2j}, θ_{3j}, and θ_{4j}; j = 1,...,NSNP, are the solution coefficients to be determined. The N_j were selected to satisfy the condition $N_j(NP_i) = \delta_{ij}$ where the Kronecker delta, δ_{ij}, is defined by $\delta_{ij} = 1$ for i = j, and $\delta_{ij} = 0$ for $i \neq j$. As a result, θ_{1j}, θ_{2j}, θ_{3j} and θ_{4j} are the values ψ_1, ψ_2, ψ_3 and ψ_4 at the nodal points (i.e., $\psi_{ij}(\eta,\varepsilon,t) = \theta_{ij}(t)$).

Area interpolation functions (shown in Figure C.1) were used as the linear basis functions which provide the necessary function continuity. As a measure of error, a residual, R_i, is defined for each field equation by,

$$R_i = \dot{\underset{\sim}{\psi}} + \Lambda_i(\psi) - \underset{\sim}{F} + \underset{\sim}{\underset{\sim}{C}}[T_c\phi]^* \qquad (C.5)$$

where Λ_i denotes the spatial operator of the ith equation and the asterisk denotes that this term appears in the carbon temperature and oxygen concentration equations only. The term arises from the reaction terms and is developed in subsection 3 of this section. The following notational convention for differentiation is adopted,

$$(\ )_i = \frac{\partial (\ )}{\partial i} \tag{C.6}$$

$$(\dot{}) = \frac{\partial (\ )}{\partial t} \tag{C.7}$$

For field equations 3.9, 3.22, 3.26 and 3.27, the residuals are,

$$R_{T_c} = (1-p)\rho_c C_c \dot{T}_c - \vec{\nabla}\cdot((1-p)(k_e)\nabla T_c) + hZ(T_c - T_a) - R_g Z \tag{C.8}$$

$$R_{T_A} = p\,\rho_a C_a \dot{T}_a - \vec{\nabla}\cdot(pk_a \nabla T_a) - hZ(T_c - T_a) + p\,\rho_a C_a(\vec{V}\cdot\vec{\nabla})T_a - (\vec{V}\cdot\vec{\nabla})pP \tag{C.9}$$

$$R_P = (p\dot{\rho}_a) - \vec{\nabla}\cdot(\frac{m}{p\mu}\nabla P) - \frac{m}{p\mu}(\nabla P\cdot\vec{\nabla})p\rho_a \tag{C.10}$$

$$R_\phi = p\dot{\phi} - \vec{\nabla}\cdot(p\,\mathcal{D}_e\,\nabla\phi) + \nabla\cdot(p\,\phi\,\vec{V}) + R_{O_2} Z \tag{C.11}$$

where the coefficients of the response variables are themselves functions of the response variables, and thus, the equations are nonlinear. In accordance with the Galerkin method, the final system of ordinary differential equations was obtained by setting each residual, R_i, orthogonal to each basis function, N_j, that is,

$$\int_{A_e} \int \underset{\sim}{N} R_i \, dA = 0 \qquad \text{(C.12)}$$

The 4*NSNP ordinary differential equations given by Equations C.12 retain the character of the original set of partial differential equations, i.e., self-adjoint operators yield symmetric matrices and non self-adjoint operators yield nonsymmetric matrices. Thus, linear field operators transform to matrix operators and nonlinear, coupled algebraic operators. Incorporation of the boundary conditions resulted in 4*NSNP nonlinear coupled ordinary differential equations,

$$F(\dot{\psi},\psi,t) = \underset{\sim}{A}\,\dot{\underset{\sim}{\psi}} + \underset{\sim}{B}\underset{\sim}{\psi} - \underset{\sim}{F} + \overset{*}{\underset{\sim}{C}}_{ij}[\psi_{T_C}\psi_{\phi}] \qquad \text{(C.13)}$$

subject to initial conditions, where $\underset{\sim}{A}$ is a (4*NSNP)*(4*NSNP) matrix, $\underset{\sim}{B}$ is the matrix associated with the linear field operators in Expression C.5, $\underset{\sim}{F}$ is an excitation vector, $\overset{*}{\underset{\sim}{C}}_{ij}$ is a 3×9 matrix arising from a bilinear operator treatment of the reaction terms in Expressions C.8 and C.11.

Adopting the convention,

$$\psi_i = \underset{\sim}{N}^T \underset{\sim}{\theta} = \sum_{j=1}^{NSNP} N_j \theta_{ij} , \quad i = 1,4 \tag{C.14}$$

and performing an integration by parts on the second order derivatives yields,

$$\iint_{A_e} \underset{\sim}{N} R_{T_c} dA = -\phi_{\ell e} (1-p) \underset{\sim}{N}(k_e)(T_c)_n d\ell + \iint_{A_e} (1-p)(k_e) \underset{\sim}{N}_r (T_c)_r dA$$

$$- \iint_{A_e} \frac{(1-p)}{r} \underset{\sim}{N}(k_e) dA + \iint_{A_e} (1-p)(k_e) \underset{\sim}{N}_z (T_c)_z dA$$

$$-\phi_{\ell e} (1-p)(k_e) \underset{\sim}{N}(T_c)_n dA + \iint_{A_e} hZ \underset{\sim}{N}(T_c - T_a) dA$$

$$- \iint_{A_e} R_g Z \underset{\sim}{N} dA + \iint_{A_e} p \rho_c \underset{\sim}{N} \dot{T}_c dA \tag{C.15}$$

$$\iint_{A_e} \underset{\sim}{N} R_{T_a} \, dA = \oint_{\ell e} pk_a \underset{\sim}{N} (T_a)_n \, d\ell + \iint_{A_e} pk_a \underset{\sim}{N}_r (T_a)_r \, dA$$

$$- \iint_{A_e} \frac{pk_a}{r} \underset{\sim}{N} (T_a)_r \, dA + \iint_{A_e} pk_a \underset{\sim}{N}_z (T_a)_z \, dA$$

$$- \oint_{\ell e} pk_a \underset{\sim}{N} (T_a)_n \, d\ell - \iint_{A_e} hZ \underset{\sim}{N} (T_c - T_a) \, dA$$

$$- \iint_{A_e} up \underset{\sim}{N} (P)_r \, dA - \iint_{A_e} u \frac{\partial p}{\partial r} \underset{\sim}{N} P \, dA$$

$$- \iint_{A_e} vp \underset{\sim}{N} (P)_z \, dA - \iint_{A_e} v \frac{\partial p}{\partial z} \underset{\sim}{N} P \, dA$$

$$+ \iint_{A_e} p \rho_a C_a u \underset{\sim}{N} (T_a)_r \, dA + \iint_{A_e} p \rho_a C_a v \underset{\sim}{N} (T_a)_z \, dA$$

$$+ \iint_{A_e} p \rho_a C_a \underset{\sim}{N} \dot{T}_a \, dA \qquad \text{(C.16)}$$

$$\iint_{A_e} \underset{\sim}{N} R_p dA = -\oint_{\ell e} \frac{m}{p\mu} \underset{\sim}{N}(P)_n d\ell + \iint_{A_e} \frac{\rho_a m}{\mu} \underset{\sim}{N}_r(P)_r dA$$

$$- \iint_{A_e} \frac{\rho_a m}{\mu r} \underset{\sim}{N}(P)_r dA - \oint_{\ell e} \frac{\rho_a m}{\mu} \underset{\sim}{N}(P)_n d\ell$$

$$+ \iint_{A_e} \frac{\rho_a m}{\mu} \underset{\sim}{N}_z(P)_z dA + \iint_{A_e} \frac{m}{p\mu} \frac{\partial p\rho_a}{\partial r} \underset{\sim}{N}(P)_r dA$$

$$+ \iint_{A_e} \frac{m}{p\mu} \frac{\partial p\rho_a}{\partial z} \underset{\sim}{N}(P)_z dA + \iint_{A_e} \frac{p}{RT_a} \underset{\sim}{N} \dot{P} dA \qquad \text{(C.17)}$$

$$\iint_{A_e} \underset{\sim}{N} R_\phi dA = -\oint_{\ell e} p\mathcal{D}_e \underset{\sim}{N}(\phi)_n d\ell + \iint_{A_e} p\mathcal{D}_e \underset{\sim}{N}_r(\phi)_r dA$$

$$- \iint_{A_e} \frac{p\mathcal{D}_e}{r} \underset{\sim}{N}(\phi)_r dA - \oint_{\ell e} p\mathcal{D}_e \underset{\sim}{N}(\phi)_n d\ell + \iint_{A_e} p\mathcal{D}_e \underset{\sim}{N}_z(\phi)_z dA$$

$$+ \iint_{A_e} pu \underset{\sim}{N}(\phi)_r dA + \iint_{A_e} pv \underset{\sim}{N}(\phi)_z dA + \iint_{A_e} \frac{(rpu)_r}{r} \underset{\sim}{N}\phi dA$$

$$+ \iint_{A_e} (pv)_z \underset{\sim}{N}\phi dA + \iint_{A_e} R_{O_2} \underset{\sim}{Z}\underset{\sim}{N} dA + \iint_{A_e} p\underset{\sim}{N}\dot{\phi} dA \qquad \text{(C.18)}$$

The line integral terms in each expression above are boundary terms which permit incorporation of natural boundary conditions.

Implementation of the boundary conditions is presented in Section 2 of this appendix. The coefficients in Equations C.15, C.16, C.17 and C.18 are temperature dependent properties, and were taken as the average values of the properties over an element. In the limit, as the elements get smaller (i.e., NSNP $\rightarrow \infty$), the average values of the coefficients converge to the exact values. Inspection of expressions C.15, C.16, C.17 and C.18 yields the six operators,

$$\iint_{A_e} \underset{\sim}{N}(\psi)_r \, dA \tag{C.19}$$

$$\iint_{A_e} \underset{\sim}{N}(\psi)_z \, dA \tag{C.20}$$

$$\iint_{A_e} \underset{\sim}{N}_r(\psi)_r \, dA \tag{C.21}$$

$$\iint_{A_e} \underset{\sim}{N}_z(\psi)_z \, dA \tag{C.22}$$

$$\iint_{A_e} \underset{\sim}{N}\psi \, dA \quad \text{and} \quad \iint_{A_e} \underset{\sim}{N}\dot{\psi} \, dA \tag{C.23}$$

$$\oint_{\ell e} \underset{\sim}{N}(\psi)_n \, d\ell \tag{C.24}$$

To formulate these operators, the global linear shape function, N_j, are defined on the local level by,

$$\underset{\sim}{N}^T\underset{\sim}{\theta} \rightarrow \underset{\sim}{\xi}^T\underset{\sim}{\theta} \tag{C.25}$$

where the natural coordinates ξ_1, ξ_2 and ξ_3 are defined by Figure C.2,

$$\xi_i = \frac{A_i}{A_e}, \quad i = 1,2,3 \tag{C.26}$$

and A_e is the area of the elemnet and the A_i are the areas (in Figure C.2) subtended by lines from a point P(r,z) inside the triangle to the triangle's vertices (r_j,z_j, $j = 1,2,3$). The local shape functions (i.e., the elements) have the following properties,

$$\psi_{ij} = \theta_{ij} \cdot \xi_j \quad ; \quad i = 1,4, \quad j = 1,3 \tag{C.27}$$

$$\xi_i(NP_j) = \delta_{ij} \; ; \quad i = 1,3, \quad j = 1,3 \tag{C.28}$$

Having defined the local shape functions, the elemental matrix operations C.19 through C.24 are,

$$\iint_{A_e} \underset{\sim}{N}(\psi)_r \, dA = \frac{1}{6}[b_j]\underset{\sim}{\theta}_{elt} \tag{C.29}$$

$$\iint_{A_e} \underset{\sim}{N}(\psi)_z \, dA = \frac{1}{6}[c_j]\underset{\sim}{\theta}_{elt} \tag{C.30}$$

$$\iint_{A_e} \underset{\sim}{N}_r(\psi)_r \, dA = \frac{1}{4A_e}[b_i b_j]\underset{\sim}{\theta}_{elt} \tag{C.31}$$

$$\iint_{A_e} \underset{\sim}{N}_z(\psi)_z \, dA = \frac{1}{4A_e}[c_i c_j]\underset{\sim}{\theta}_{elt} \tag{C.32}$$

$$\iint_{A_e} \underset{\sim}{N}\psi \, dA = \frac{A_e}{12}[k]\underset{\sim}{\theta}_{elt}, \quad \begin{matrix} k = 1, \; i \neq j \\ k = 2, \; i = j \end{matrix} \tag{C.33}$$

$$\oint_{\ell e} k\underset{\sim}{N}(\psi)_n \, d\ell = \oint_{\ell e} k\underset{\sim}{N}(\psi)_r \, dr - \oint_{\ell e} k\underset{\sim}{N}(\psi)_z \, dz \tag{C.34}$$

where a(i,j) coefficients of the element matrices A(3 × 3) are given by,

$$a(i,j) = [g] \; ; \quad g = g(i,j) \tag{C.35}$$

and the vector $\underset{\sim}{\theta}_{elt}$ is given by,

$$\underset{\sim}{\theta}_{elt} = \begin{bmatrix} \theta_1 \\ \theta_2 \\ \theta_3 \end{bmatrix} \tag{C.36}$$

The derivations of these operators are presented in Section A.5 of this appendix.

2. Implementation of Boundary Conditions

Having formulated the system matrices for the field equations, treatment of the boundary conditions is now discussed. Each field equation is treated individually.

a. Porous Solid Energy (Heat Transfer) Equation

There are three types of boundary conditions that can occur: Dirichlet, Neumann and Cauchy (mixed) boundary conditions. The treatment of each is as follows. For Dirichlet boundary conditions, one may specify an equation to be a linear equation (i.e., independent of time) by placing a 1 on the diagonal of the system stiffness matrix corresponding to the particular degree of freedom at hand and setting each time derivative matrix coefficient for the same equation equal to zero. An alternative scheme involves setting the time derivative diagonal term equal to one and setting all stiffness coefficients (in the same equation) equal to zero. In this manner one specifies the Dirichlet value as an initial condition whose residual is identically zero and thus is invariant with time. Treatment of Neumann boundary conditions is as follows,

$$\oint_{\ell e} k\nabla\chi d\xi = \oint_{\ell e} \rho\, d\xi \rightarrow -\frac{\bar{\rho}_{\ell e}}{2} \text{ added to local F(1) and local F(2) at the element nodal points} \qquad \text{(C.37)}$$

In the above expression, χ is a response variable and ρ is an average value of flux across an element. Treatment of

Cauchy boundary conditions is as follows,

$$\oint_{\ell e} k\nabla\chi d\xi = \oint_{\ell e} k(\chi - \chi_\infty) \rightarrow \bar{k}_{\ell e} \frac{\ell e}{3} \begin{bmatrix} 2 & 1 \\ 1 & 2 \end{bmatrix} \begin{bmatrix} \chi_1 \\ \chi_2 \end{bmatrix}$$

scattered into $\underset{\sim}{\beta}$ and $-\bar{K}_{\ell e} \frac{\ell e}{2}$ added to

F(1) and F(2) at the element nodal points

(C.38)

For a complete development of the theory for incorporating boundary conditions, see [Ref. 28].

3. Treatment of the Reaction Rate Term

An exponential reaction rate term appears in both the porous solid and oxygen diffusion equation. The reaction expression is,

$$R_c = A \phi^n \exp(-E/R_u \hat{T}_c) \tag{C.39}$$

In the carbon equation, Expression C.39 appears as,

$$R_g Z = (R_c \Delta H_R) Z \tag{C.40}$$

In the oxygen concentration equation, Expression C.39 appears as,

$$R_{O_2} Z = (R_c f_R^{-1}) Z \tag{C.41}$$

The reaction rate term may be treated in various ways.

a. Treatment as an Excitation (Force Term)

This treatment is the easiest of all schemes. The term is merely evaluated at the last time step and is assumed to be constant over the next integration time step, i.e.,

$$R_c = \{A R_{O_2}^n \exp(E/R_u \hat{T}_c)\}^* \qquad (C.42)$$

The superscript * indicates evaluation occurring at the previous time step. The value of the term is evaluated at the ith nodal point and inserted as a factor in the corresponding carbon energy or the oxygen diffusion equation of the ith nodal point.

b. Linear Operator Treatment of O_2 Concentration

In order to realize an improvement over the first treatment, one may retain a portion of the reaction expression as an operator by making the following rearrangement:

$$R_c = \{A R_{O_2}^n \phi^{n-1} \exp(-E/R_u \hat{T}_c)\}^* \cdot [\phi] \qquad (C.43)$$

where $[\phi]$ denotes a spatial operator treatment of the response variable.

c. Temperature and O_2 Concentration Bilinear Operator Treatment of the Reaction Rate Term

The bilinear operator treatment of the reaction rate is the present method of treatment. The reaction rate

term is rearranged as follows,

$$R_c = \frac{A R_{O_2}^{n} \; {}^{n-1}\exp(-E/R_u T_c)}{T_c} * [T_c \phi] \qquad (C.44)$$

Letting

$$T_c = \underset{\sim}{\xi}^T \underset{\sim}{\theta}_1 \qquad (C.45)$$

and

$$\phi = \underset{\sim}{\xi}^T \underset{\sim}{\theta}_4 \qquad (C.46)$$

and invoking natural coordinates [Ref. 28], an elementally averaged contribution results in the following area integral,

$$\underset{\sim}{C} = \underset{\sim}{\overline{C}} \iint_{A_e} \underset{\sim}{\xi} \; \underset{\sim}{\xi}^T \; \underset{\sim}{\theta}_1 \; \underset{\sim}{\xi}^T \; \underset{\sim}{\theta}_4 \; dA \qquad (C.47)$$

Expanding yields,

$$\underset{\sim}{C} = \overline{C} \iint \underset{\sim}{\xi}^T < \xi_1\xi_j \,\vdots\, \xi_2\xi_j \,\vdots\, \xi_3\xi_j > (\theta_{1i} \cdot \theta_{4j}) \; ; \qquad (C.48)$$

$$i = 1,3, \quad j = 1,3$$

A final explicit expansion of the integral looks like,

$$\underset{\sim}{C} = \bar{C} \left[\begin{array}{ccc:ccc:ccc} \xi_1^3 & \xi_1^2\xi_2 & \xi_1^2\xi_3 & \xi_1^2\xi_2 & \xi_1\xi_2^2 & \xi_1\xi_2\xi_3 & \xi_1^2\xi_3 & \xi_1\xi_2\xi_3 & \xi_1\xi_3^2 \\ \xi_1^2\xi_2 & \xi_1\xi_2^2 & \xi_1\xi_2\xi_3 & \xi_1\xi_2^2 & \xi_2^3 & \xi_2^2\xi_3 & \xi_1\xi_2\xi_3 & \xi_2^2\xi_3 & \xi_2\xi_3^2 \\ \xi_1^2\xi_3 & \xi_1\xi_2\xi_3 & \xi_1\xi_3^2 & \xi_1\xi_2\xi_3 & \xi_2^2\xi_3 & \xi_2\xi_3^2 & \xi_1\xi_3^2 & \xi_2\xi_3^2 & \xi_3^2 \end{array}\right] \qquad (C.49)$$

Invoking the integral formula of natural coordinates [Ref. 28],

$$\iint_{A_e} \xi_1^a \, \xi_2^b \, \xi_3^c \, dA = \frac{a!b!c!2A_e}{(a+b+c+2)!} \qquad (C.50)$$

results in,

$$\underset{\sim}{C} = \frac{\bar{C}A_e}{60} \left[\begin{array}{ccc:ccc:ccc} 6 & 2 & 2 & 2 & 2 & 1 & 2 & 1 & 2 \\ 2 & 2 & 1 & 2 & 6 & 2 & 1 & 2 & 2 \\ 2 & 1 & 2 & 1 & 2 & 2 & 2 & 2 & 6 \end{array}\right] (\underset{\sim}{T}_c\underset{\sim}{\phi}) \qquad (C.51)$$

where,

$$\bar{C} = \left\{ \frac{A \, Z \, R_{O_2}^n \, \phi^{n-1} \exp(-E/R_u \hat{T}_c)}{T_c} (\Delta H_R \text{ or } f_R^{-1}) * \right\} \qquad (C.52)$$

The asterisk denotes as applicable for T_c or ϕ equations.

4. Implementation of Reaction Term in the Numerical Method

Franke's (modified Gear) integration routine requires a calculation of (or an approximation to) the Jacobian matrix

from the system matrices, $\underset{\sim}{A}(t)$, $\underset{\sim}{B}(t)$ and $\underset{\sim}{C}(t)$. In order to include effects of T_c and ϕ arising from reaction rate terms in the Jacobian vector, and thereby improve the efficiency of the integration routine, the combustion terms are incorporated into the residual equations (in DIFMOD). Modifications to the Jacobian matrix are accomplished in the JACMOD and NUITSL routines. Reaction rate terms of Expressions C.40 and C.41 contribute nine terms to the respective residual equations and twenty-seven terms to the Jacobian vector. Reaction terms are generally expressed as,

$$RT = \sum_{i=1}^{3} \sum_{j=1}^{3} C_{ik}(\psi_{1i}\psi_{4j}) , \quad k = 1,9 \tag{C.53}$$

The Jacobian is defined as,

$$J \equiv \frac{\partial F(\dot{\psi},\psi,t)}{\partial \dot{\psi}} + \frac{\partial F}{\partial \psi}(\dot{\psi},\psi,t) \tag{C.54}$$

Contributions arising from RT as a result of $\partial F/\partial \psi$ are,

$$\frac{\partial RT}{\partial \psi_{1i}} = \sum_{j=1}^{3} C_{ik^*}\ \psi_{4j} \tag{C.55}$$

where the k* are compatible with the column locations in the C matrix of the ψ_{1i} products, and

$$\frac{\partial RT}{\partial \psi_{4j}} = \sum_{i=1}^{3} C_{ik^*} \psi_{1i} \qquad (C.56)$$

where the k* are compatible with the column locations in the C matrix of the ψ_{4j} products. Terms from Equation C.55 may be incorporated into the PW Jacobian vector (containing contributions to the Jacobian from the linear spatial operators) as contributions from Equation C.8 with combustion. Similarly, terms from Equation C.56 may be incorporated into PW for terms arising from the O_2 residual equations with combustion. The remaining contributions to the Jacobian vector, Equation C.56 for the carbon equations and terms arising from Equation C.55 for the O_2 equations are stored in the PWMOD (NDOF/2,9) matrix. The column number or variable of differentiation array, INMOD (NDOF/2,9) and PWMOD array are communicated to the NUITSL routine so additional Jacobian terms not assimilated into the PW array (by virtue of the storage scheme selected) may be taken into account during the convergence sequence for the new iterates. The iterating scheme is of Newton-Raphson type. Thus, the final synthesis of the Jacobian including effects of all terms arising from combustion is consummated.

5. Derivation of the FEM Operators

In the section on the finite element formulation, the following six differential operators were identified,

$$\iint_{A_e} \underset{\sim}{N}(\psi)_r \, dA \tag{C.57}$$

$$\iint_{A_e} \underset{\sim}{N}(\psi)_z \, dA \tag{C.58}$$

$$\iint_{A_e} \underset{\sim}{N}_r(\psi)_r \, dA \tag{C.59}$$

$$\iint_{A_e} \underset{\sim}{N}_z(\psi)_z \, dA \tag{C.60}$$

$$\iint_{A_e} \underset{\sim}{N}(\psi) \, dA \quad \text{and} \quad \iint_{A_e} \underset{\sim}{N} \dot{\psi} \, dA \tag{C.61}$$

$$\oint_{\ell e} k\underset{\sim}{N}(\psi)_n \, d\ell \tag{C.62}$$

where N_j are the global basis functions. These operators are constructed on the element level by introducing the corresponding element basis functions, ξ_i. The global and element basis functions are related by,

$$\psi_i = \underset{\sim}{N}^T \underset{\sim}{\theta} \rightarrow \underset{\sim}{\xi}^T \underset{\sim}{\theta} \tag{C.63}$$

The derivation of the local elemental matrices (using the local coordinate system depicted in Figure C.3) according

to the Galerkin method for the global operations proceeds as follows:

For Operator C.29(also C.57),

Global	Local	
$\iint_{A_e} \underset{\sim}{N}(\psi)_r \, dA$	$\iint_{A_e} \underset{\sim}{\xi} \, \underset{r\sim}{\xi}^T \underset{\sim}{\theta} \, dA$	(C.64)

Noting that,

$$\frac{\partial \xi_j}{\partial r} = \frac{b_j \theta_j}{2A_e} \quad \text{and} \quad \frac{\partial \xi_j}{\partial z} = \frac{c_j \theta_j}{2A_e} \; ; \quad j = 1,3 \tag{C.65}$$

where the repeated index implies Einsteinian notation, the elemental matrix becomes,

$$\iint_{A_e} \underset{\sim}{\xi} \, \underset{\sim\sim\sim}{\frac{b_j^T}{2A_e}} \underset{\sim}{\theta} dA \tag{C.66}$$

Expanding,

$$\iint_{A_e} \begin{bmatrix} \xi_1 \\ \xi_2 \\ \xi_3 \end{bmatrix} \left(\frac{b_j}{2A_e}\right)^T \underset{\sim}{\theta} dA = \frac{1}{6} \begin{bmatrix} b_1 & b_2 & b_3 \\ b_1 & b_2 & b_3 \\ b_1 & b_2 & b_3 \end{bmatrix} \underset{\sim}{\theta} \tag{C.67}$$

For Operator C.30 (also C.58),

Global	Local	
$\iint_{A_e} \underset{\sim}{N}(\psi)_z \, dA$	$\iint_{A_e} \underset{\sim}{\xi} \, \underset{z\sim}{\xi}^T \underset{\sim}{\theta} dA$	(C.68)

Substituting the local shape functions gives,

$$\iint_{A_e} \underset{\sim}{\xi} \left(\frac{\underset{\sim\sim\sim}{C_j}}{2A_e}\right)^T \underset{\sim}{\theta}\, dA \tag{C.69}$$

the elemental matrix becomes,

$$\iint_{A_e} \begin{bmatrix} \xi_1 \\ \xi_2 \\ \xi_3 \end{bmatrix} \left(\frac{\underset{\sim\sim\sim}{C_j}}{2A_e}\right)^T \underset{\sim}{\theta}\, dA = \frac{1}{6} \begin{bmatrix} C_1 & C_2 & C_3 \\ C_1 & C_2 & C_3 \\ C_1 & C_2 & C_3 \end{bmatrix} \underset{\sim}{\theta} \tag{C.70}$$

For Operator C.31(also C.59)

Global	Local	
$\iint_{A_e} \underset{\sim}{N}_r(\psi)_r\, dA_e$	$\iint_{A_e} \underset{\sim}{\xi}_r \underset{\sim}{\xi}_r^T \underset{\sim}{\theta}\, dA$	(C.71)

Substituting the local shape functions gives,

$$\iint_{A_e} \frac{\underset{\sim\sim\sim}{b_i}}{2A_e} \frac{\underset{\sim\sim\sim}{b_j}^T}{2A_e} \underset{\sim}{\theta}\, dA = \frac{1}{4A_e^2} \iint_{A_e} \begin{bmatrix} b_1^2 & b_1b_2 & b_1b_3 \\ b_1b_2 & b_2^2 & b_2b_3 \\ b_1b_3 & b_3b_1 & b_3^2 \end{bmatrix} \underset{\sim}{\theta} dA \tag{C.72}$$

the elemental matrix becomes,

$$\iint_{A_e} \underset{\sim}{N}_r\,(\psi)_r\, dA = \frac{1}{4A_e} \begin{bmatrix} b_1^2 & b_1b_2 & b_1b_3 \\ b_1b_2 & b_2^2 & b_2b_3 \\ b_1b_3 & b_2b_3 & b_3^2 \end{bmatrix} \underset{\sim}{\theta} \tag{C.73}$$

For Operator C.32 (also C.60),

Global	Local	
$\iint_{A_e} \underset{\sim}{N}_z(\psi)_z \, dA$	$\iint_{A_e} \underset{\sim}{\xi}_z \, \underset{\sim}{\xi}_z^T \, \underset{\sim}{\theta} \, dA$	(C.74)

Substituting the local shape functions gives,

$$\iint_{A_e} \frac{\underset{\sim}{C}_i}{2A_e} \frac{\underset{\sim}{C}_i^T}{2A_e} \underset{\sim}{\theta} \, dA = \frac{1}{4A_e^2} \iint_{A_e} \begin{bmatrix} C_1^2 & C_1C_2 & C_1C_3 \\ C_1C_2 & C_2^2 & C_2C_3 \\ C_1C_3 & C_2C_3 & C_3^2 \end{bmatrix} \underset{\sim}{\theta} \, dA \qquad (C.75)$$

the elemental matrix becomes,

$$\iint_{A_e} \underset{\sim}{\xi}_z \, \underset{\sim}{\xi}_z^T \, \underset{\sim}{\theta} \, dA = \frac{1}{4A_e} \begin{bmatrix} C_1^2 & C_1C_2 & C_1C_3 \\ C_1C_2 & C_2^2 & C_2C_3 \\ C_1C_3 & C_2C_3 & C_3^2 \end{bmatrix} \underset{\sim}{\theta} \qquad (C.76)$$

For Operator C.33 (also C.61)

Global	Local	
$\iint_{A_e} \underset{\sim}{N} \, \psi \, dA$	$\iint_{A_e} \underset{\sim}{\xi} \, \underset{\sim}{\xi}^T \, \underset{\sim}{\theta} \, dA$	(C.77)

Substituting the local shape functions gives,

$$\iint_{A_e} \underset{\sim}{\xi}\ \underset{\sim}{\xi}^T\ \underset{\sim}{\theta}\ dA = \iint_{A_e} \begin{bmatrix} \xi_1^2 & \xi_1\xi_2 & \xi_1\xi_3 \\ \xi_1\xi_2 & \xi_2^2 & \xi_2\xi_3 \\ \xi_1\xi_3 & \xi_2\xi_3 & \xi_3^2 \end{bmatrix} \underset{\sim}{\theta}\ dA \qquad (C.78)$$

the elemental matrix becomes,

$$\iint_{A_e} \underset{\sim}{\xi}\ \underset{\sim}{\xi}^T\ \underset{\sim}{\theta}\ dA = \frac{A_e}{12} \begin{bmatrix} 2 & 1 & 1 \\ 1 & 2 & 1 \\ 1 & 1 & 2 \end{bmatrix} \underset{\sim}{\theta} \qquad (C.79)$$

The last operator C.34 (also C.62) is incorporated into the excitation vector as described in the FEM formulation and has been addressed in Subsection 2, Implementation of Boundary Conditions.

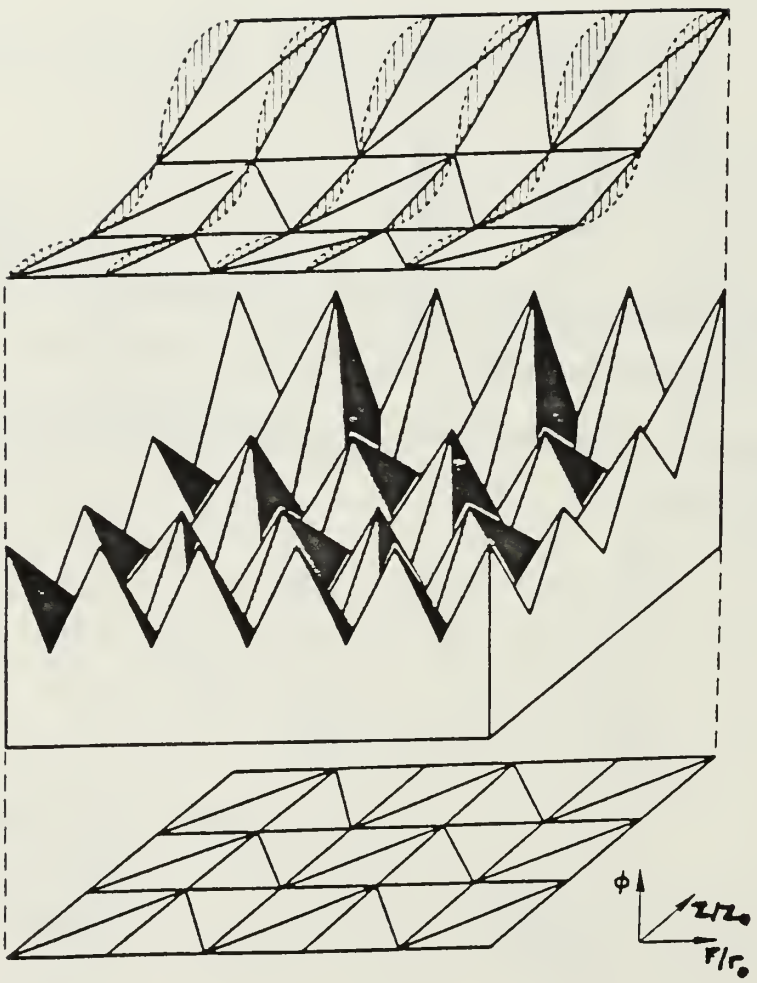

Figure C.1 Area Interpolation Functions

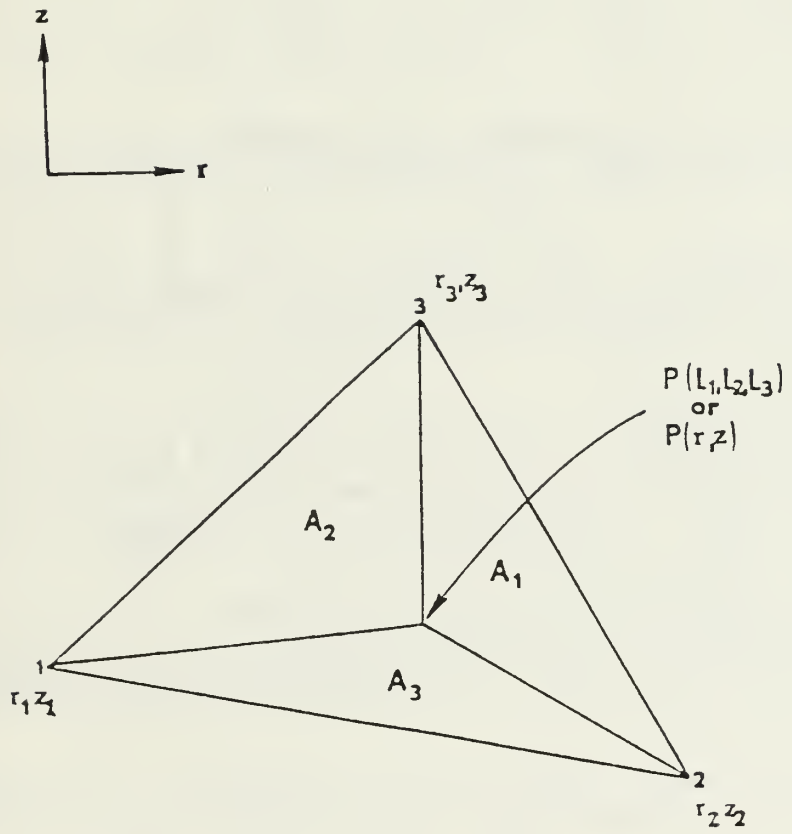

Figure C.2 Area Coordinates

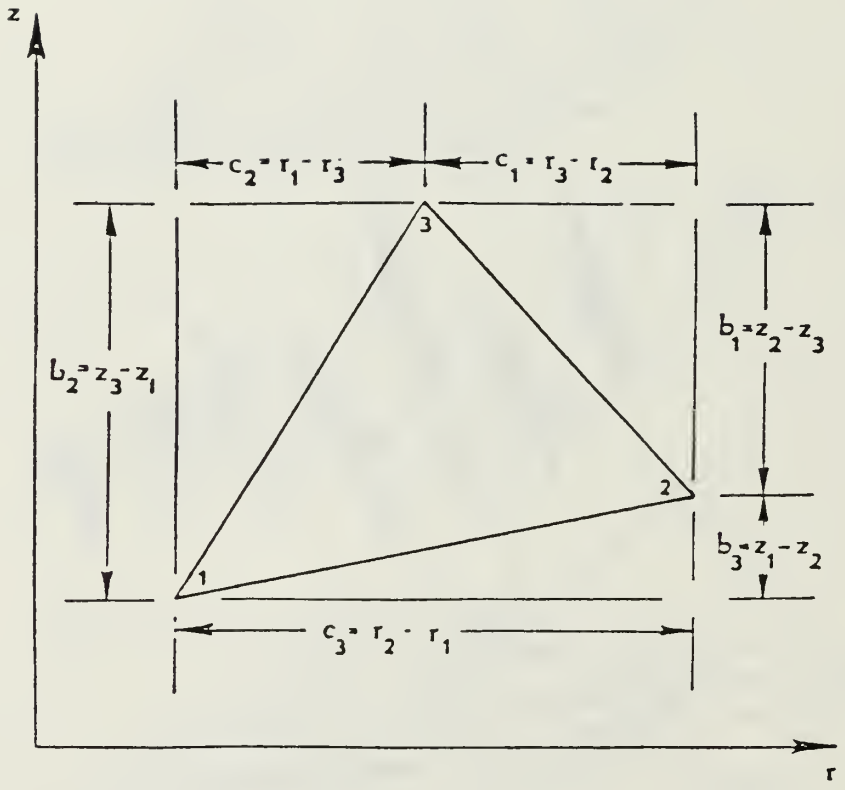

Figure C.3 Local Coordinates

LIST OF REFERENCES

1. Kordylewski, W., "Influence of Aerodynamics on the Critical Parameter s of Thermal Ignition," International Journal for Numerical Methods in Engineering, Vol. 17, pp. 1081-1091, 1981.

2. Sahota, M.S. and Pagni, P.J., "Heat and Mass Transfer in Porous Media Subject to Fires," International Journal of Heat Transfer, Vol. 22, pp. 1069-1081, 1981.

3. Mehta, P.S. and Sams, W.N. and Luss, D., "Wrong Way Behavior of PackedBed Reactors," AICHE Journal, Vol. 27, pp. 234-246, March 1981.

4. Kim, C.S. and Chung, P.M., "An Asymptotic, Thermo-Diffusive Ignition Theory of Porous Solid Fuels," Journal of Heat Transfer, pp. 269-275, May 1976.

5. Saatdijan, E. and Caltagirone, J.P., "Natural Convection in Porous Layer Under the Influence of an Exothermic Decomposition," Transactions of the ASME, Vol. 102, pp. 654-658, November 1980.

6. Horne, R.N. and O'Sullivan, M.J., "Convection in a Porous Media Heated from Below: the Effect of Temerature Dependent Viscosity and Thermal Expansion Coefficient," Transactions of the ASME, Vol. 100, pp. 448-452, August 1978.

7. Hickox, C.E., "Thermal Convection at Low Rayleigh Number from Concentrated Sources in Porous Media," Transactions of the ASME, Vol. 103, pp. 232-236, May 1981.

8. Chan, Y.T., "Analysis of Transient Three Dimensional Convection in Porous Media," Transactions of the ASME, Vol. 103, pp. 242-248, May 1981.

9. Vatikiotis, C., Heat Transfer Model of Flow Through a Porous Medium, Doctoral Thesis, Naval Postgraduate School, 1982.

10. Scheidegger, A.E., The Physics of Flow Through Porous Media, University of Toronto Press, Toronton, 1974.

11. Carman, P.C., Flow of Gases Through Porous Media, Academic Press, London, 1956.

12. Boffa, C.C., "Experimental Gas Flow Characteristics in Transpiration Cooled Matrices," 5th Int'l Heat Transfer Conf., Tokyo, Japan, Proceedings, 5, September 1974.

13. Frank-Kamenetskii, D.A., Diffusion and Heat Transfer in Chemical Kinetics, Plenum Press, New York, 1969.

14. Vulis, L.A., Thermal Regimes of Combustion, McGraw-Hill Book Co., New York, 1961.

15. Parker, A.S. and Hottel, H.C., "Combustion Rate of Carbon," Ind. and Eng. Chem., 28, November 1936, pp. 1334-1341.

16. Arthur, J.A., "Reactions Between Carbon and Oxygen," Trans. Faraday Soc., 47, 1951, pp. 164-178.

17. Janaf Thermochemical Tables, 2nd Edition, Dow Chemical Company, 1970.

18. Smoot, D.L., and Pratt, D.T., Pulverized Coal Combustion and Gasification, Plenum Press, New York, 1979.

19. Green, D.W., and Perry, R.H., Heat Transfer with a Flowing Fluid Through Porous Media, Chem. Eng. Prog. Symp., Series No. 32, 57, 1961, pp. 61-68.

20. Sundaresan, S. and Amundson, N.R. and Rutherford, A., "Observations on Fixed Bed Dispersion Models: The Role of the Interstitial Fluid," AICHE Journal, 26, July 1980, pp. 529-536.

21. Riaz, M., "Analytical Solutions for Single-and-Two-Phase Models of Packed-Bed Thermal Storage Systems," J. of Heat Transfer, 99, August, 1977, pp. 489-492.

22. Mendelsohn, A.R., "Transient Temperature of a Porous-Cooled Wall," AIAA Journal, 1, June 1963, pp. 1449-1451.

23. Schneider, P.J., and Brogan, J.J., "Temperature Response of a Transpiration-Cooled Plate," ARS Journal, February 1962, pp. 233-236.

24. Russel, H.W., "Principles of Heat Flow in Porous Insulators," Am. Ceramic Soc. J., 18, 1935, pp. 1-5.

25. White, F.M., Heat Transfer, Addison-Wesley Publishing Company, 1984.

26. Heisler, M.P., "Temperature Charts for Induction and Constant Temperature Heating," ASME Transactions, Vol. 69, 1947, pp. 227-236.

27. Schneider, P.J., Conduction Heat Transfer, Addison-Wesley, Reading, Mass., 1955.

28. Zienkiewicz, O.C., The Finite Element Method in Engineering Science, McGraw Hill, 1971.

29. Franke, R., and Salinas, D., "An Efficient Method for Solving Stiff Transient Field Problems Arising from FEM Formulations," Comp. & Maths. with Appls., Vol. 6, pp. 15-21, Pergamon Press Ltd., 1980.

30. Franke, R., "Integration Scheme for Systems of Stiff Differential Equations," Naval Postgraduate School, Monterey, Ca., 1978.

31. Denbigh, D.K., and Turner, J.C.R., Chemical Reactor Theory, Cambridge Press, London, 1971.

32. Roshenow, W.M., and Hartnett, J.P., Handbook of Heat Transfer, McGraw-Hill Book Co., New York, 1973.

33. Yoshida, F., Ramaswami, D., and Houugen, D.A., "Temperature and Partial Pressures at the Surfaces of Catalyst Particles," A. I. Ch. E. Journal, 8, 1962.

34. Gilliland, E.R., "Diffusion Coefficients in Gaseous Systems," Ind. Eng. Chem., 26, 1934, p. 681.

35. Holman, J.P., Heat Transfer, McGraw-Hill Book Co., New York, 1976.

36. Kays, W.M. and Crawford, M.E., Convective Heat and Mass Transfer, 2nd Edition, McGraw-Hill Book Co., p. 327, 1980.

37. Fontenot, J.S., Graphite-Epoxy Composite Material Response to Carrier Deck Fire, Naval Weapons Center, NWC Technical Memorandum 3351, November 1979.

INITIAL DISTRIBUTION LIST

		No. Copies
1.	Defense Technical Information Center Cameron Station Alexandria, Virginia 22314	2
2.	Library, Code 0142 Naval Postgraduate School Monterey, California 93943	2
3.	Department Chairman, Code 69 Department of Mechanical Engineering Naval Postgraduate School Monterey, California 93943	2
4.	Professor David Salinas, Code 69Zc Department of Mechanical Engineering Naval Postgraduate School Monterey, California 93943	5
5.	LT Ben Martinez Production Department Pearl Harbor Naval Shipyard Pearl Harbor, Hawaii 96860	5

13375

210397

Thesis
M35922 Martinez
c.1 Two-D heat transfer
through porous media
with heat generation.

210397

Thesis
M35922 Martinez
c.1 Two-D heat transfer
through porous media
with heat generation.

thesM35922
Two-D heat transfer through porous media
3 2768 002 12832 4
DUDLEY KNOX LIBRARY